Small Molecule Assembly Modulators with Pan-Cancer Therapeutic Efficacy

Authors: Anuradha F. Lingappa[#1], Olayemi Akintunde[#1], Connie Ewald[1], Markus Froehlich[1], Niloufar Ziari[1], Shao Feng Yu[1], Maya Michon[1], Suguna Mallesh[1], Jim Lin[1], Anatoliy Kitaygorodskyy[1], Dennis Solas[1], Jonathan C. Reed[2], Jaisri R. Lingappa[2] Andreas Mueller-Schiffmann[3], Carsten Korth[3], Dharma Prasad[1], Aysegul Nalca[4], Emily Ashton[5], Brad Fabbri[5], Emma Petrouski[1], Debendranath Dey[1], David Andrews[6], and Vishwanath R. Lingappa[1,7]

Affiliations:

[1]Prosetta Biosciences, San Francisco, CA USA

[2] Dept. of Global Health, University of Washington, Seattle, WA, USA.

[3]Institute of Neuropathology, Heinrich Heine University, Dusseldorf, Germany

[4]United States Army Medical Research Institute for Infectious Diseases, Fredrick MD, USA

[5]TechAccel, Overland Park, KS, USA

[6]Sunnybrook Research Institute, Toronto, ON, Canada

[7]University of California, San Francisco, CA, USA

[#]Co-first authors who contributed equally to this work

*To whom correspondence should be addressed vlingappa@prosetta.com

Abstract:

Two structurally-unrelated small molecule chemotypes, represented by compounds PAV-617 and PAV-951, with antiviral activity in cell culture against monkeypox virus (MPXV) and human immunodeficiency virus (HIV) respectively, were studied for anti-cancer efficacy. Each exhibited apparent pan-cancer cytotoxicity, reasonable pharmacokinetics, and non-toxicity in mice at active concentrations. Anti-tumor properties of each compound were validated in mouse xenografts against A549 human lung cancer. The targets of these compounds are unconventional: each binds to a different transient, energy-dependent multi-protein complex containing the protein KAP-1(TRIM28), an allosteric modulator known to broadly regulate mechanisms underlying viral and nonviral disease states including cancer. Treatment with these compounds alters the target multi-protein complexes in a manner consistent with allosteric modulation as their mechanism of action. These compounds appear to remove a block, crucial for cancer survival and progression, on the homeostatic linkage of uncontrolled cellular proliferation to apoptosis. These compounds may provide starting points for development of next-generation non-toxic, cancer therapeutics.

41 **Introduction**

42 The similarity of the interactions of viral infection and cancer with the healthy host has often
43 been noted (Javier and Butel, 2008). Both represent pathological processes of extremely diverse origin,
44 that overcome the complex feedback controls of homeostasis, to the detriment of the host (Morales-
45 Sánchez and Fuentes-Pananá, 2014). Both exploit natural selection as a powerful weapon to overcome
46 host defenses. Viruses have done so over deep evolutionary time through co-evolution with their hosts
47 and through the emergence of resistance mutation in response to the selective pressure of treatments
48 (Ison, 2011; Kaján et al., 2020). Cancers regularly use the latter mechanism, resulting in clonal mutants
49 that drive cancer progression (Usman et al., 2021).

50 At least seven different viruses— Epstein-Barr virus (EBV), hepatitis B virus (HBV), hepatitis C
51 virus (HCV), human T-lymphotropic virus 1 (HTLV-1), human papillomavirus (HPV), Kaposi sarcoma-
52 associated herpesvirus (KSHV or HHV-8), and Merkel cell polyomavirus (MCPyV)— are known to be
53 directly oncogenic through their alteration of the cellular environment and/or impairment of the host's
54 innate immune system defenses (Cirone, 2018; Krump and You, 2018). It has therefore been proposed
55 that the study of viruses could play a key role in the discovery of new cancer treatments by identifying
56 cellular targets that drive tumorigenesis (O'Shea, 2005).

57 The incompleteness in our current understanding of the dynamics of host homeostasis and its
58 myriad of feedback controls has been a disadvantage for efforts to design novel therapeutic
59 countermeasures against both viruses and cancer. However, a recent unconventional approach to
60 antiviral drug discovery has identified host allosteric sites essential for homeostasis that are repurposed
61 by viral infection (Müller-Schiffmann et al., 2022). The antiviral compounds identified by this approach
62 appear to restore key features essential to host homeostasis (Müller-Schiffmann et al., 2022). We
63 wished to determine whether those compounds might have therapeutic applicability against cancer,

64 given the analogy in how both viruses and cancers drive departure from homeostasis. The results to be
65 presented here suggest this is the case and shed light on molecular pathways relevant for both viral and
66 neoplastic disease, providing a strategy for development of novel cancer therapeutics.

67 Utilizing a cell-free protein synthesis and assembly (CFPSA) system, a library of approximately
68 150,000 drug-like small molecules was screened for compounds which blocked the assembly of viral
69 capsids without inhibiting host protein synthesis (Broce et al., 2016; U. F. Lingappa et al., 2013; Müller-
70 Schiffmann et al., 2022; Reed et al., 2021). The hit compounds identified have been termed "*assembly*
71 *modulators*" (Müller-Schiffmann et al., 2022, 2021a). A collection of 300 structurally-diverse assembly
72 modulators were assembled from hits demonstrating activity against capsid assembly in one or more
73 viral family (V. Lingappa et al., 2013). Antiviral assembly modulators from this collection have been
74 validated against live virus in cell culture for multiple viral families including *Retroviridae*, *Rhabdoviridae*,
75 *Poxviridae*, *Adenoviridae*, *Herpesviridae*, *Paramyxoviridae*, *Coronaviridae*, *Orthomyxoviradae*, and
76 *Picornaviridae* (U. F. Lingappa et al., 2013; Müller-Schiffmann et al., 2022, 2021b; Priyamvada et al.,
77 2021; Reed et al., 2021). In two cases, *Coronaviridae* (porcine epidemic diarrhea virus) and
78 *Paramyxoviridae* (respiratory syncytial virus), cellular antiviral activity has been confirmed in animal
79 disease models (Müller-Schiffmann et al., 2022).

80 These antiviral assembly modulators appear to target host-viral protein-protein interactions via
81 allosteric sites that control repurposing of host assembly machinery for viral capsid formation and which
82 also allow disengagement of host innate immune defenses such as autophagy (Müller-Schiffmann et al.,
83 2022). In one study, a class of assembly modulators was shown to change the composition of a
84 transient, energy-dependent multi-protein complex whose components include p62/SQSTM1, a key
85 regulator of autophagy (Müller-Schiffmann et al., 2022). This multi-protein complex is co-opted upon
86 viral infection to lose p62/SQSTM1 and to gain the viral nucleoprotein (Müller-Schiffmann et al., 2022).
87 Upon treatment with an antiviral assembly modulator, the multi-protein complex is restored to its

88 normal composition, with loss of the viral nucleoprotein component and re-engagement of
89 p62/SQSTM1 (Müller-Schiffmann et al., 2022).

90 The discovery of dynamic multi-protein complexes whose composition changes with drug
91 treatment offers a new means of parsing out post-translational protein heterogeneity and its relevance
92 for diseased states. The amount of a given protein that has been observed in the multi-protein
93 complexes targeted by antiviral assembly modulators comprises only a very small fraction of the total
94 amount of the component proteins present in a cell (Müller-Schiffmann et al., 2022). The role played by
95 the small subset of the particular proteins that are part of the particular complex may be related to
96 "moonlighting" functions observed for a growing set of cellular and viral proteins (Copley, 2012; Jeffery,
97 2019, 2018).

98 We hypothesized that if an overlap between viral and oncogenic pathways exists, some antiviral
99 assembly modulators might be capable of disrupting multi-protein complexes associated with the
100 hallmarks of cancer (Hanahan and Weinberg, 2011, 2000). To test the hypothesis, we established a
101 cancer-relevant counterscreen and applied it to previously-identified assembly modulating compounds.
102 In this paper, we describe two assembly modulators which were originally characterized for their
103 antiviral properties but are now shown to have potential as cancer therapeutics based on *in vivo*
104 screening and *in vitro* validation studies.

105

106

107

108

109

110 **Results**

111 Uncontrolled cellular proliferation: a hallmark of cancer inhibited by assembly modulators PAV-617 and
112 PAV-951

113 No hallmark of cancer is more fundamental than uncontrolled proliferation (Hanahan and
114 Weinberg, 2000). Uncontrolled proliferation normally triggers cell death mechanisms, including
115 apoptosis (Pucci et al., 2000). Therefore, to survive, a cancer must achieve a means of evading cell death
116 long enough to complete cell division and reset the cell death timer. This, in turn, allows further
117 proliferation, during which time additional mutations can occur and selection pressure will drive higher
118 and higher grade malignancy and, ultimately, metastasis (Pfeffer and Singh, 2018). Compounds capable
119 of arresting proliferation, either directly or indirectly, could make potent anti-cancer agents because the
120 delay in cancer progression would provide an opportunity for a patient's innate immune system and
121 other homeostatic mechanisms to re-establish themselves.

122 Abnormal signaling pathways triggered by aberrant protein-protein interactions is one way that
123 neoplastic cells are able to achieve uncontrolled proliferation (Pfeffer and Singh, 2018). In order to
124 characterize whether assembly modulators could arrest the proliferation of neoplastic cells by
125 redirecting key protein-protein interactions, we first sought to identify a cell line in which endogenous
126 apoptosis was substantially lacking. While a successful anti-cancer compound would likely exhibit both
127 anti-proliferative and cytotoxic efficacy, we wanted to conduct our screen under conditions where a
128 readout measuring the arrest of proliferation would not be obscured by downstream activation of the
129 normal cascade of events comprising cell death pathways.

130 We assessed caspase-3/7 activity in multiple tumor cell lines with an Apo-ONE assay (see **Fig.**
131 **1A**). The expected correlation between endogenous triggers of apoptotic cell death and cancer
132 progression was demonstrated in the LNCaP prostate cancer progression cell model, where LNCaP-C33

133 early (hormone sensitive) cancer cells displayed substantially more markers of apoptosis than LNCaP-
134 C81 late (hormone resistant) cancer cells (Igawa et al., 2002). In the Apo-ONE assay, CHO K1 cells show
135 very little endogenous apoptosis (see **Fig. 1A**). Hennes-20, a CHO K1 derivative into which the human
136 APP751 V717F mutation has been stably transfected, show even less apoptosis than their parental line
137 (see **Fig. 1A**).

138 We then counterscreened our collection of anti-viral assembly modulator in Hennes-20 cells
139 plated at low (500 cells/well) versus high (15,000 cells/well) densities and treated with DMSO (vehicle)
140 or dose-titration of compounds. The rationale for this screen is that an intrinsically toxic compound
141 should kill cells regardless of density, including in Hennes-20 cells. A compound that selectively triggers
142 the arrest of proliferation will appear cytotoxic due to inhibition of cell growth when plated at a low
143 density. However, it will appear non-toxic to cells plated at a high density where the cells are
144 approaching confluence and the readout detected by a cell viability assay is already close to the
145 maximum.

146 Two structurally-unrelated small molecules (Tanimoto similarity score of 41%), PAV-617 and
147 PAV-951, displayed the desired phenotype (see **Figs. 1B** and **1C**). Our findings in Hennes-20 cells at low
148 versus high density comparison suggested that the effect of these compounds in cells lacking
149 endogenous apoptosis was due to inhibition of proliferation.

150 To confirm that the drug-induced inhibition observed in low density Hennes 20 cells resulted
151 from temporary arrest of proliferation and not cell death, compound was removed after a period of
152 treatment (24 hour for PAV-617 and 6 hours for PAV-951), and cell growth was measured over the
153 subsequent two weeks for recovery potential. The cells treated with PAV-617 and PAV-951 initially
154 showed reduced cell density relative to the control, but once compound was removed, growth was

155 restored over time (See **Figs. 1D** and **1E**). By day 11, cell density in compound-treated cells caught up to

156 the DMSO-treated cells (See **Figs. 1D** and **1E**).

157 Since Hennes 20 cells do not appear to have endogenous apoptosis, we sought to use a different

158 cancer cell line to assess whether that inhibition of proliferation would be accompanied by cell death.

159 The recovery experiment was conducted in LNCaP C-33 cells which appear to have substantial

160 endogenous apoptosis (see **Fig. 1A**), and treatment with PAV-617 and PAV-951 did inhibit cancer cell

161 growth relative to the DMSO-treated control but the cells did not recover or grow significantly once

162 compound was removed (See **Figs. 1F** and **1G**).

163

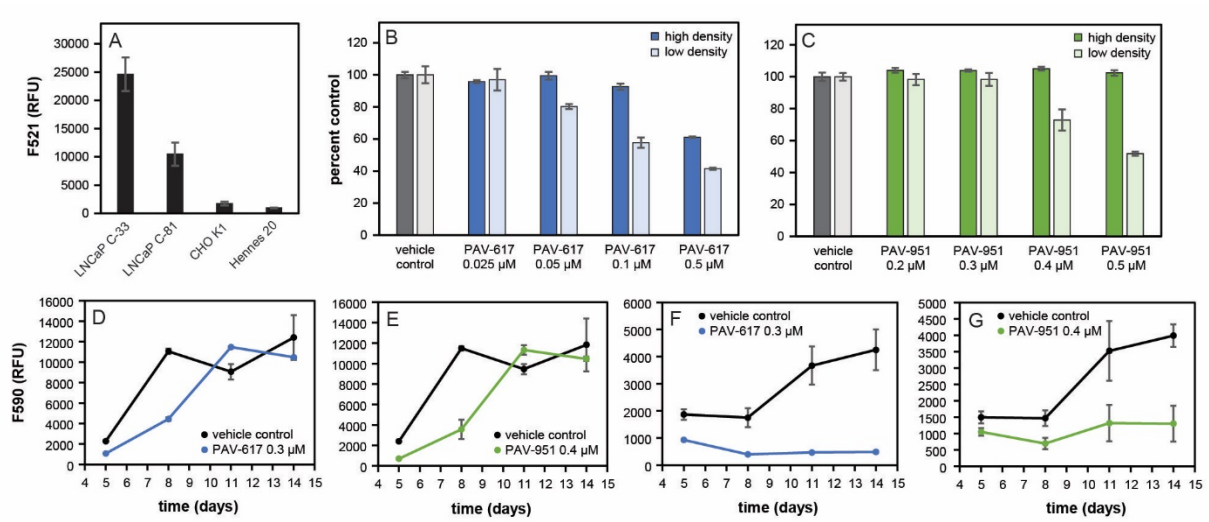

164

165 **Figure 1. Assay development and activity of hit compounds PAV-617 and PAV-951. Fig. 1A** shows

166 assessment of the endogenous apoptosis response in multiple cell lines. Plates were seeded with LNCaP

167 C-33, LNCaP C-81, CHO K-1, and Hennes 20 cells. After three days of growth Apo-ONE reagent was added

168 and caspase-3/7 activity was determined by fluorescent readout. Averages and standard deviation of

169 observed activity in triplicate-repeated samples were calculated and graphed in Microsoft Excel. The

170 Hennes 20 cell line was chosen for the counterscreen based on its low levels of caspase activity. **Figs. 1B**

171 **and 1C** show activity of PAV-617 and PAV-951 in the assay, where parallel plates of Hennes 20 cells were

172 seeded at a high density of 15,000 cells per well and a low density of 500 cells per well and treated with
173 DMSO, PAV-617, or PAV-951 in triplicate-repeated dose titrations. Fluorescent reading (RFU)
174 corresponding to cell viability was calculated using an alamarBlue™ assay and the averages and standard
175 deviations for triplicate-repeated samples were calculated and graphed on Microsoft Excel as a
176 percentage of the DMSO-treated cells. PAV-617 exhibited dose-dependent inhibition of cell growth in the
177 low density plate, indicating an EC50 between 0.1uM and 0.5uM. PAV-617 exhibited some toxicity to cells
178 at the higher doses tested, indicating a CC50 slightly greater than 0.5uM. PAV-951 exhibited dose-
179 dependent inhibition of cell growth in the low-density plate, indicating an EC50 around 0.5uM. PAV-951
180 exhibited no significant inhibition of cell growth at the tested doses in the high-density plate, indicating a
181 CC50 greater than 0.5uM. **Figs. 1D- 1G** show recovery of cancer cell growth following removal of
182 compound. Hennes 20 or LNCaP C-33 cells were seeded at a low density then incubated with DMSO, PAV-
183 617, or PAV-951. After a period of treatment, the medium containing compound was removed and
184 replaced with fresh media. Plates were assessed for cell viability by alamarBlue™ on days 5, 8, 11, and 14
185 and the averages and standard deviations of triplicate-repeat samples were calculated and graphed over
186 time on Microsoft Excel. PAV-617 and PAV-951 treated Hennes 20 and LNCaP C-33 cells all showed
187 reduced viability compared to matched DMSO-treated cells on day 5. However, cell growth in the Hennes
188 20 cells which had been treated with compound recovered with time, while the LNCaP C-33 cells which
189 had been treated with compound did not recover.

190

191 <u>Investigating the activities of PAV-617 and PAV-951: from modulators of viral capsid assembly to pan-</u>
192 <u>cancer therapeutics</u>

193 The anti-proliferative compounds PAV-617 and PAV-951 had originally emerged from our CFPSA
194 screen as inhibitors of viral capsid formation. The CFPSA model had been validated by demonstrating
195 that hit antiviral assembly modulators display activity against infectious viruses in cell culture (U. F.
196 Lingappa et al., 2013; Müller-Schiffmann et al., 2022; Priyamvada et al., 2021; Reed et al., 2021). PAV-

197 617 is active against pox viruses in cell culture (see **Fig. 2A** for MPXV activity and Priyamvada et al., 2021
198 for chickenpox activity). The effective concentration for half maximal activity (EC50) of PAV-617 against
199 MPXV is approximately 300 nM (See **Fig. 2A**). PAV-951 is active against HIV in cell culture with an EC50
200 between 1 uM and 300 nM (see **Fig. 2B**).

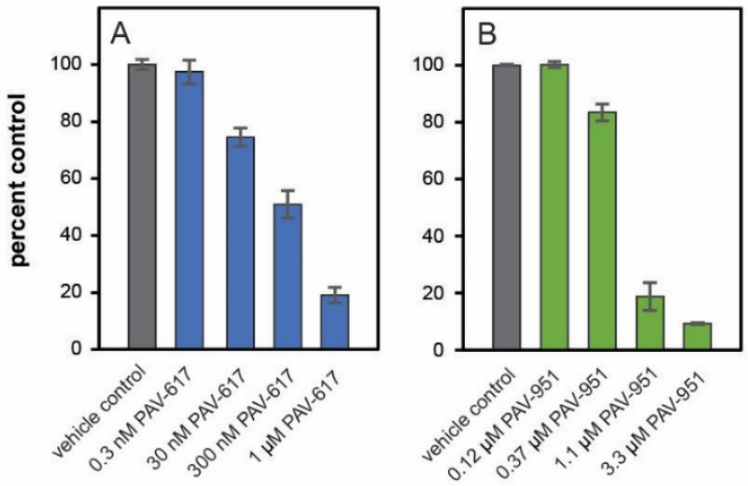

201

202 **Figure 2. Anti-viral and pharmacokinetic properties of PAV-617 and PAV-951. Fig. 2A** shows activity of
203 PAV-617 against MPXV. BSC-40 cells were infected with 100 plaque forming units of MPXV Zaire 79
204 andtreated with PAV-617 for three days. Averages and standard deviation for plaques observed with
205 triplicate-repeated dose-titration of PAV-617 are shown as a percentage of the plaques observed in
206 untreated cells with an EC50 of approximately 300 nM. **Fig. 2B** shows activity of PAV-951 against HIV. MT-
207 2 cells were infected with NL4-3 Rluc HIV and treated with PAV-951 for four days. Averages and standard
208 deviation of viral titer observed with triplicate-repeated dose-titration of PAV-951 are shown as a
209 percentage of the titer observed in DMSO-treated cells, with an EC50 between 0.37 uM and 1.1 uM.

210

211 When PAV-617 and PAV-951 were identified as having anti-cancer activity in addition to anti-
212 viral properties, we suspected that the compounds might correct cancer-induced defects in protein
213 assembly that were related to the aberrant assemblies induced by viruses. To get a better

214 understanding of how the defects present themselves across diverse cancers, we assessed the anti-
215 cancer activity of these two compound chemotypes on a panel of 15 cancer cell lines from the Eurofins
216 OncoPanel™ ("OncoPanelTM Cell-Based Profiling Service Details," n.d.). The cell lines were derived from
217 a variety of tissues and were representative of male and female patients of different ages from pediatric
218 to senior. Both PAV-617 and PAV-951 showed pan-cancer activity with dose-dependent tumor growth
219 inhibition in all 15 cell lines (see **Figs. 3A** and **3B**).

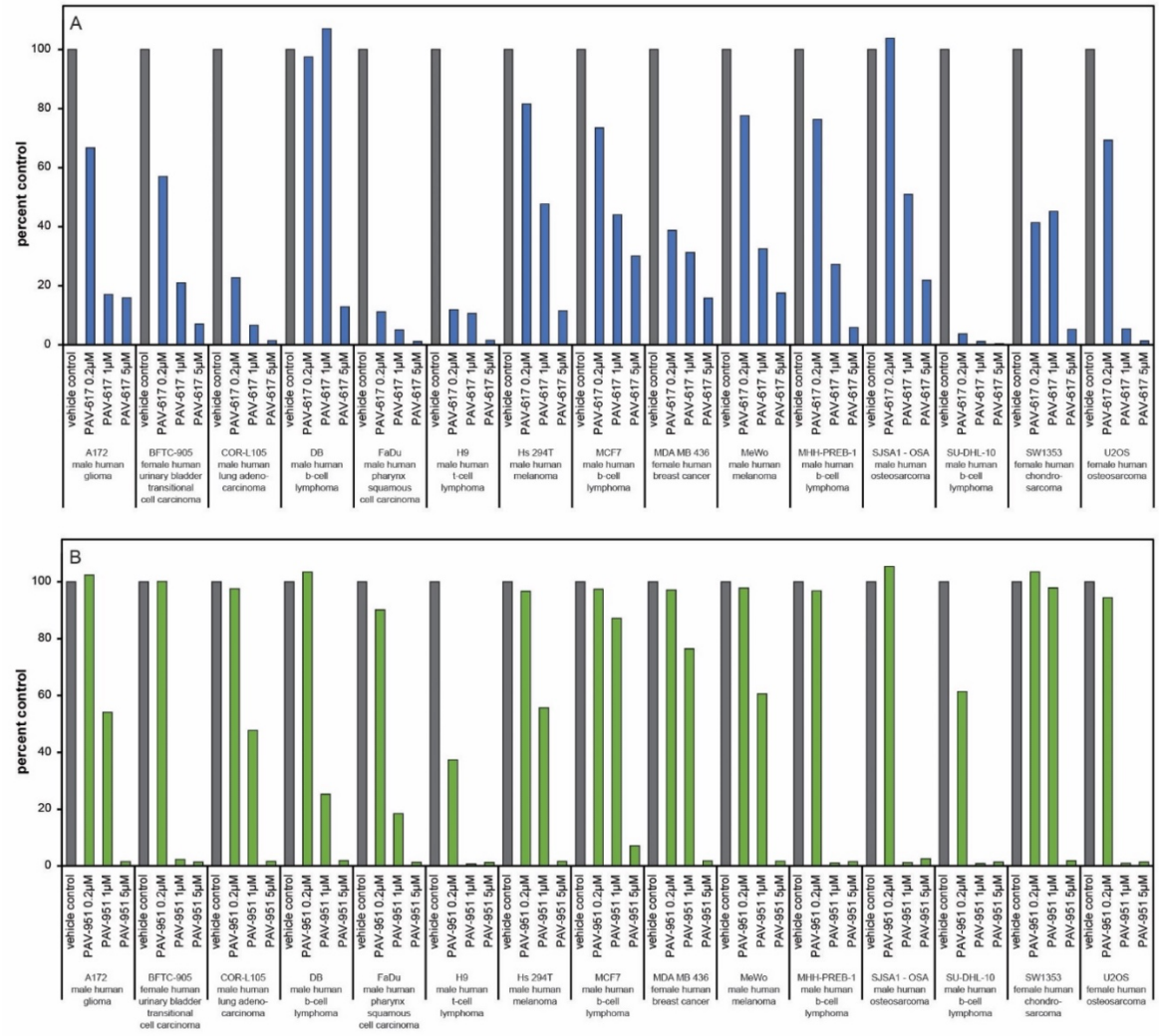

220

221 **Figure 3. Pan-cancer activity of PAV-617 and PAV-951. Figs. 3A** and **3B** show results from a panel of
222 human tumor cell lines— A172 (male human glioma), BFTC-905 (female human urinary bladder

223 transitional cell carcinoma), COR-L105 (male human lung adenocarcinoma), DB (male human b-cell
224 lymphoma), FaDu (male human pharynx squamous cell carcinoma), H9 (male human t-cell lymphoma), Hs
225 294T (male human melanoma), MCF7 (female human breast cancer), MDA MB 436 (female human breast
226 cancer), MeWo (male human melanoma), MHH-PREB-1 (male human b-cell lymphoma), SJSA1-OSA (male
227 human osteosarcoma), SU-DHL-10 (male human b-cell lymphoma), SW1353 (female human
228 chondrosarcoma), and U-2 OS (female human osteosarcoma). Cells were grown for 24 hours then treated
229 with either vehicle, PAV-617, or PAV-951. Cell viability after 3 days of treatment was measured as
230 bioluminescence intensity and averages of triplicate-repeat dose-titrations with PAV-617 and PAV-951
231 were graphed on Microsoft Excel as percent of bioluminescence observed in DMSO-treated cells. Both
232 compounds showed inhibitory effects in all 15 cell lines.

233

234 Animal validation of PAV-617 and PAV-951 anti-cancer efficacy

235 With demonstrated anti-viral activity, demonstrated anti-cancer activity, and data supporting a
236 proliferation-based mechanism of action, we assessed mouse toxicology and pharmacokinetic (PK)
237 properties in order to determine suitability for efficacy studies in an animal model.

238 The maximum tolerated dose (MTD) estimates how much compound can be administered to an
239 animal without adverse effects (Gad, 2014). When administered orally to mice, both PAV-617 and PAV-
240 951 displayed MTDs greater than 20 mg/kg, which was the highest dose tested, as no clinical symptoms
241 or significant differences were observed between vehicle and treatment groups. When administered by
242 intraperitoneal (IP) injection, the MTD of PAV-617 was determined to be greater than 10 mg/kg, which
243 was the highest dose tested. When administered by IP injection, the MTD of PAV-951 was determined to
244 be 2.5 mg/kg because at the next-highest dose (5 mg/kg), one animal displayed dullness, a clinical sign
245 of toxicity, for 24 hours. The animal subsequently recovered and behaved normally for the remaining

246 48-hour observation period and no abnormality was observed at necropsy for any animals in the PAV-
247 951 5 mg/kg or 10 mg/kg treatment groups.

248 The PK properties are based on the absorption, distribution, metabolism, and excretion of a
249 compound in a living organism and are necessary to determine dosing parameters because any
250 compound designed for clinical use needs to achieve an efficacious concentration in a target organ
251 (Hughes et al., 2011; Reichel and Lienau, 2015). As an early measure of PK, we determined the
252 concentration of compound in the plasma of rats or mice over time following one intravenous (IV), one
253 IP dose, or one oral dose. Both compounds were detectable in the animals through all administration
254 routes, though the maximum concentration achieved (Cmax) and rate of elimination were variable
255 across conditions (see **Supplemental Fig. 1**).

256 We determined that, while both chemical series would need optimization on the PK and
257 toxicologic properties before being named as clinical drug-candidates, PAV-617 and PAV-951 would be
258 adequate for a preliminary animal efficacy study in order to validate whether or not the anti-
259 proliferative properties of the compounds observed in cell culture translates to anti-proliferative
260 properties in animals.

261 In the animal efficacy study, human A459 non-small cell lung cancer cells were grafted
262 subcutaneously onto mice. After 30 days of tumor establishment, the animals received daily treatment
263 with PAV-617 or PAV-951 and tumor volume was measured over time. The doses and routes of
264 administration for PAV-617 (10 mg/kg IP injection) and PAV-951 (1.5 mg/kg IV injection) were
265 determined based on their MTD and PK properties (see **Supplemental Fig. 1**). The PAV-617 study was
266 conducted for 28 days and the PAV-951 study was conducted for 14 days. As negative and positive
267 controls, both studies included a group treated with vehicle only and a group treated with Gemcitabine
268 Hydrochloride, an FDA-approved drug for non-small cell lung cancer ("Reference ID" 4433223-

269 Accessdata.fda.gov," n.d.). The Gemcitabine was administered at a dose of 100 mg/kg twice weekly.

270 Both PAV-617 and PAV-951 reduced tumor growth significantly compared to the vehicle-only groups

271 and performed comparably to Gemcitabine despite being administered at substantially lower doses (See

272 **Figs. 4A** and **4B**).

273

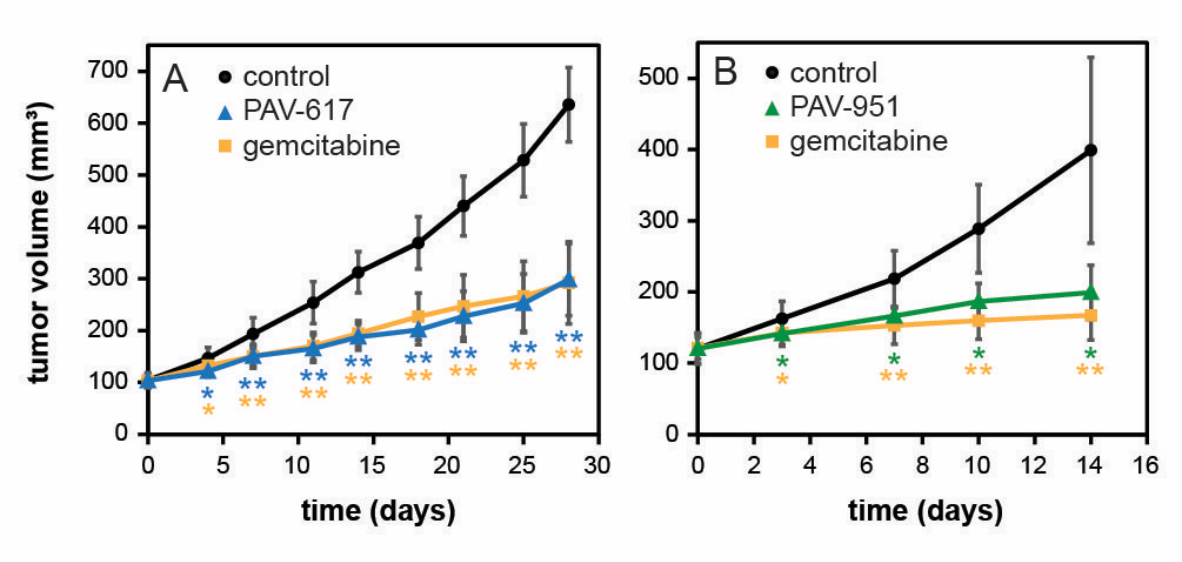

274

275 **Figure 4) Anti-proliferative activities of PAV-617 and PAV-951 in animal xenograft model.** Female nude

276 mice were injected with 0.1 mL a suspension containing 1 x 10^6 A549 cells. Tumor volume was initially

277 measured after 30 days. Subsequently randomized groups containing 6 animals each began receiving

278 treatment with vehicle, PAV-617, PAV-951, or Gemcitabine ("Reference ID" 4433223-

279 Accessdata.fda.gov," n.d.). The tumor volumes of animals within each treatment group were measured

280 over time. **Fig. 4A** shows tumor volume across time in the PAV-617 study where one treatment group

281 received daily doses of vehicle, one treatment group received daily doses of 10 mg/kg PAV-617, and one

282 treatment group received twice weekly doses of 100 mg/kg Gemcitabine for 28 days. After 28 days of

283 treatment, the Gemcitabine treated animals had a tumor volume that was, on average, 46% of tumor

284 volume found in the vehicle-treated animals and PAV-617-treated animals had a tumor volume that was,

285 on average, 47% of the tumor volume found in the vehicle-treated animals. **Fig. 4B** shows tumor volume

286 across time in the PAV-951 study where one treatment group received daily doses of vehicle, one
287 treatment group received daily doses of 1.5 mg/kg PAV-951, and one treatment group received twice
288 weekly doses of Gemcitabine for 14 days. After 14 days of treatment, the Gemcitabine treated animals
289 had a tumor volume that was, on average, 42% of tumor volume found in the vehicle-treated animals and
290 PAV-951-treated animals had a tumor volume that was, on average, 50% of the tumor volume found in
291 the vehicle-treated animals. Statistical significance is indicated with ** where the p value is < 0.01 and *
292 where the p value is < 0.05.

293

294 Characterizing the targets of PAV-617 and PAV-951

295 As PAV-617 and PAV-951 were identified by a phenotypic screen, their actual targets were unknown
296 during the early stages of compound advancement. To identify their targets, each molecule was coupled
297 to affigel resins from a position on the molecule unrelated to proliferation arrest activity based on
298 structure-activity-relationship (SAR) exploration. In that way, they could serve as target-binding ligands
299 for drug resin affinity chromatography (DRAC) (Tanaka, 2009). LNCaP C-33 cells were chosen for DRAC
300 starting material because we knew PAV-617 and PAV-951 displayed efficacy against them and we
301 wanted a model for our target engagement studies that would account for mechanisms of endogenous
302 apoptosis and innate immune system responses. Extracts were prepared from LNCaP C-33 cells that
303 were treated for 22 hours with either DMSO, PAV-617, or PAV-951. The extracts were applied to the
304 PAV-617, PAV-951, or control drug resins, washed with 100 bed volumes of buffer, and eluted with
305 either 100uM of PAV-617 or 100uM of PAV-951.

306 Samples of the DRAC eluate were sent for analysis by tandem mass spectrometry (MS-MS). The
307 DRAC eluate from the PAV-617 and PAV-951 resins contained large sets of proteins missing from the
308 control resin eluate. This included cancer-implicated proteins from the literature (see Figs. **5A**, **5B**, and
309 **5C**). 92 proteins from the DMSO-treated cell extracts were identified in the PAV-617 resin eluate that

310 were not present in the control resin eluate. 116 proteins from the DMSO-treated cell extracts were
311 identified in the PAV-951 resin eluate which were not present in the control resin eluate. Of the proteins
312 identified by MS-MS as unique or greatly enriched in the drug resin eluates, 38 proteins in the DMSO-
313 treated cell extracts were unique to PAV-617 (see **Fig. 5A**), 62 proteins in the DMSO-treated cell extracts
314 were unique to PAV-951 (see **Fig. 5B**), and 54 proteins from the DMSO-treated cell extracts were found
315 in both the PAV-617 and PAV-951 resin eluates (see **Fig. 5C**). When the proteins detected in the eluates
316 were searched in a database for cancer-implicated proteins, 23 of the proteins from the PAV-617 resin
317 eluate and 29 proteins from the PAV-951 resin eluate were known to be part of cancer-relevant
318 interactomes (see **Figs. 5A**, **5B**, and **5C**).

319 The MS-MS indicated that when LNCaP C-33 cells were treated with compound, composition of
320 the eluate was subsequently affected. For both the PAV-617 and the PAV-951 resin eluates, the spectral
321 counts of some particular proteins detected by MS-MS increased or decreased in treatment conditions
322 (see **Figs. 5A**, **5B**, and **5C**). However, for other proteins, the number of spectral counts detected in the
323 eluates remained unchanged upon treatment (see **Figs. 5A**, **5B**, and **5C**).

324

A

gene name	control resin eluate	DMSO treated cells PAV-617 resin/PAV-617 eluate	PAV-617 treated cells PAV-617 resin/PAV-617 eluate	DMSO treated cells PAV-951 resin/PAV-951 eluate	PAV-951 treated cells PAV-951 resin/PAV-951 eluate
CCT3	0	14	8	0	0
CCT7	0	11	18	0	0
IVD	0	10	13	0	0
TCP1	0	6	5	0	0
CLPP	0	5	6	0	0
BLVRB	0	5	4	0	0
TIMM13	0	5	4	0	0
NUCKS1	0	4	3	0	0
ACADS	0	4	5	0	0
TUBB4B	0	4	2	0	0
RPS12	0	3	0	0	0
MTHFD1	0	3	0	0	0
DHRS4	0	3	3	0	0
OLA1	0	3	4	0	6
PTBP1	0	3	2	0	0
PSME1	0	3	0	0	0
ACADSB	0	3	2	0	0
SND1	0	3	2	0	0
PHPT1	0	2	0	0	0
RPS28	0	2	2	0	0
ARG2	0	2	2	0	0
TRNT1	0	2	3	0	0
EIF4A1	0	2	0	0	0
EIF5A	0	2	2	0	0
HNRNPL	0	2	5	0	0
LDHB	0	2	5	0	0
MARCKSL1	0	2	5	0	0
ACADM	0	2	4	0	0
MAT2B	0	2	0	0	0
FKBP3	0	2	0	0	0
RACK1	0	2	0	0	0
STOML2	0	2	0	0	0
BTF3	0	2	0	0	0
TCOF1	0	2	0	0	0
HADHA	0	2	0	0	0
TUBA1B	0	2	3	0	2
VAPB	0	2	0	0	0
XRCC6	0	2	0	0	0

2 — 18
spectral count

B

gene name	control resin eluate	DMSO treated cells PAV-617 resin/PAV-617 eluate	PAV-617 treated cells PAV-617 resin/PAV-617 eluate	DMSO treated cells PAV-951 resin/PAV-951 eluate	PAV-951 treated cells PAV-951 resin/PAV-951 eluate
MAOA	0	0	0	19	17
FECH	0	0	2	14	15
CKB	0	0	0	13	2
ST13	0	0	0	13	11
DLD	0	0	2	12	6
ACSL1	0	0	0	11	5
HEXB	0	0	0	9	4
CTSD	0	0	0	9	5
EIF4B	0	0	0	8	6
PYCR1	0	0	6	8	5
SARS	0	0	0	8	10
HSPE1	0	0	0	6	3
LYPLAL1	0	0	0	6	7
RDH11	0	0	2	6	2
ATP5I	0	0	0	5	5
CLIC1	0	0	0	5	4
ACOT13	0	0	0	4	4
ATP5L	0	0	0	4	2
ATP5O	0	0	0	4	4
NDUFA4	0	0	0	4	2
KHSRP	0	0	3	4	4
ILF2	0	0	0	4	0
LETM1	0	0	0	4	4
PCBP2	0	0	6	4	0
PDE12	0	0	0	3	7
ATP5B	0	0	0	3	2
NTPCR	0	0	0	3	2
CTNNA1	0	0	0	3	2
COX5B	0	0	0	3	2
HSP90B1	0	0	0	3	2
SDR39U1	0	0	0	3	0
HNRNPA3	0	0	4	3	0
KRT18	0	0	0	3	0
NCL	0	0	0	3	2
HSD17B4	0	0	0	3	0
CHCHD2P9	0	0	2	3	0
SSBP1	0	0	0	3	3
SLIRP	0	0	2	3	2
RPS21	0	0	0	2	0
SLC25A5	0	0	0	2	0
ATP5D	0	0	0	2	2
ATP5E	0	0	0	2	3
CACYBP	0	0	0	2	0
CBR4	0	0	0	2	3
CLIC4	0	0	0	2	0
CMC1	0	0	0	2	0
DNAJB11	0	0	0	2	0
DNAJC3	0	0	0	2	4
EIF3A	0	0	0	2	0
HNRNPH3	0	0	0	2	3
HARS	0	0	0	2	0
IMPDH2	0	0	0	2	3
TIMM8B	0	0	0	2	0
ME2	0	0	0	2	0
NDUFA8	0	0	0	2	0
SNU13	0	0	0	2	0
PABPN1	0	0	0	2	0
PPOX	0	0	0	2	3
RALA	0	0	0	2	2
SCFD1	0	0	0	2	4
SQRDL	0	0	0	2	4
VDAC1	0	0	0	2	0

2 — 19
spectral count

C

gene name	control resin eluate	DMSO treated cells PAV-617 resin/PAV-617 eluate	PAV-617 treated cells PAV-617 resin/PAV-617 eluate	DMSO treated cells PAV-951 resin/PAV-951 eluate	PAV-951 treated cells PAV-951 resin/PAV-951 eluate
HSPD1	0	121	135	13	10
HSPA8	0	26	34	66	64
HSPA5	0	10	11	72	60
EEF1A1	0	17	16	43	32
PDIA3	0	37	46	20	18
ATP5A1	0	20	29	33	24
HSPA9	0	23	37	22	21
HSPA1A	0	9	17	35	23
PHGDH	0	21	18	16	10
ACTG1	0	25	23	11	12
HNRNPU	0	10	2	24	11
HNRNPK	0	17	14	15	10
PRDX3	0	10	12	19	16
TUFM	0	13	14	15	7
PRDX1	0	15	13	12	6
STIP1	0	15	23	8	3
CCT4	0	16	22	6	6
HNRNPA2B1	0	8	9	13	10
NPM1	0	11	14	10	8
ACADVL	0	2	2	18	14
NADK2	0	5	5	15	13
CS	0	9	17	11	12
CCT2	0	11	11	9	7
ECH1	0	4	4	15	11
MRPL12	0	4	7	14	12
HNRNPM	0	10	12	6	8
PRDX2	0	10	15	6	0
HSPB1	0	14	20	2	0
PA2G4	0	10	7	5	3
HSD17B10	0	5	9	6	4
EEF2	0	5	3	6	6
SRP9	0	2	0	8	5
HNRNPA1	0	5	17	5	4
FKBP4	0	7	8	3	3
PCBP1	0	7	7	3	2
PTGES2	0	2	0	7	6
HSDL2	0	5	8	4	2
TRIM28	0	5	2	4	6
TUBB	0	5	0	4	0
ALDOA	0	2	6	6	7
HNRNPD	0	3	5	5	3
NARS	0	4	2	4	2
PPIB	0	6	2	2	3
ECI2	0	2	0	5	4
SHMT2	0	3	9	4	7
RAN	0	2	4	4	0
HNRNPH2	0	2	4	4	2
HNRNPC	0	2	3	4	0
YARS	0	3	2	3	6
DARS2	0	2	5	3	0
CIRBP	0	2	2	3	0
RDH13	0	2	0	3	0
AIFM1	0	2	3	2	2
CCT6A	0	2	6	2	0

2 — 135
spectral count

Figure 5. Identification of proteins in PAV-617 and PAV-951 resin eluates by MS-MS. DRAC experiments were performed where 30 ul of DMSO or compound-treated LNCaP cell extract, adjusted to a protein concentration of approximately 10 mg/ml in column buffer, was incubated on a column containing 30ul of affigel resin coupled to either PAV-617, PAV-951, or a 4% agarose matrix (control) for one hour at 4 degrees Celsius. The input material flow-through was collected and the resin was washed with 3 mL

331 column buffer then eluted overnight at 4 degrees Celsius in 100 ul of either 100uM PAV-617 or 100uM
332 PAV-951 in column buffer. **Figs. 5A-5C** show spectral counts of proteins detected by MSMS in single-point
333 DRAC eluates. **Fig. 5A** shows the set of proteins only detected in PAV-617 resin eluate. **Fig. 5B** shows the
334 set of proteins only detected in the PAV-951 resin eluate. **Fig 5C.** shows the set of proteins detected in
335 both the PAV-617 and the PAV-951 resin eluates. Conditional formatting has been applied where relative
336 abundance (by spectral count) of a given protein in a sample is visualized on a yellow-to-black scale**.**
337 Proteins implicated with cancer in the Bushman labs oncogene database
338 (http://www.bushmanlab.org/links/genelists) have been indicated in red.

339

340 When we entered the proteins identified from the DRAC eluate into a database of protein-
341 protein interactions, we discovered that many of the proteins eluted by either or both PAV-617 or PAV-
342 951 were known to be involved in networks that involved frequent interactions and associations with
343 each other (see **Supplemental Fig. 2**).

344 DRAC experiments were conducted side-by-side in triplicate with and without addition of
345 metabolic energy by running the experiment at 4 degrees Celsius versus 22 degrees Celsius and
346 supplementing with an "energy cocktail" of ribonucleotide triphosphates (1mM rATP, 1mM rGTP, 1mM
347 rCTP, 1mM rUTP), and 5 ug/mL creatine kinase. Changes in the amounts of proteins that bound and
348 eluted with PAV-617 or PAV-951 were observed by western blot in the presence of these metabolic
349 energy substrates (see **Figs. 6A** and **6B**). For the PAV-617 resin eluate, B-tubulin (TUBB), KRAB-
350 associated protein 1 (KAP1 also known as TRIM28), Methylenetetrahydrofolate dehydrogenase 1
351 (MTHFD1), and protein disulfide isomerase (PDI)— proteins which had previously been identified in the
352 eluate by MS-MS— all showed up by western blot in larger amounts under energy conditions (see **Fig.**
353 **6A**). For the PAV-951 resin eluate, MTHFD1, PDI, and heterogenous ribonucleoprotein K (hnRNPK) were
354 observed to be enhanced under energy conditions (see **Fig. 6B**). To the contrary, the amount of KAP1

355 identified in the PAV-951 resin eluate decreased in the presence of metabolic energy substrates (see **Fig.**
356 **6B**).

357 To confirm that the enrichment required the combination of metabolic energy substrates and
358 compound rather than the presence of energy substrates alone, resins were eluted side-by-side in
359 triplicate with either PAV-617, PAV-951, or 1% DMSO all containing the energy cocktail. By western blot,
360 eluates from both PAV-617 and PAV-951 resins were found to contain significant amounts of KAP1,
361 MTHFD1, and PDI relative to the control resin or DMSO elution (see **Figs. 6C and 6D**). The eluate of PAV-
362 617 resin contained TUBB which the PAV-951 resin eluate did not have in any greater amount than the
363 control (see **Figs. 6C and 6D**). The eluate of PAV-951 resin contained hnRNPK, not present in the PAV-
364 617 resin eluate in greater amount than the control (see **Figs. 6C and 6D**).

365 DRAC experiments were conducted under conditions where the starting extract was prepared
366 from LNCaP C-33 cells that had been treated with DMSO, 100 uM PAV-617, or 100 uM PAV-951 for 24
367 hours in order to see if the changes to the eluate observed by MS-MS would repeat with energy
368 supplementation (see **Fig. 5**). Western blots of triplicate-repeated samples showed the PAV-617 resin
369 eluate contained increased amounts of KAP1 and decreased amounts of TUBB when cells were treated
370 with PAV-617, meanwhile PAV-951 resin eluate showed decreased amounts of both KAP1 and hnRNPK
371 when cells were treated with PAV-951 (see **Figs. 6E** and **6F**).

372

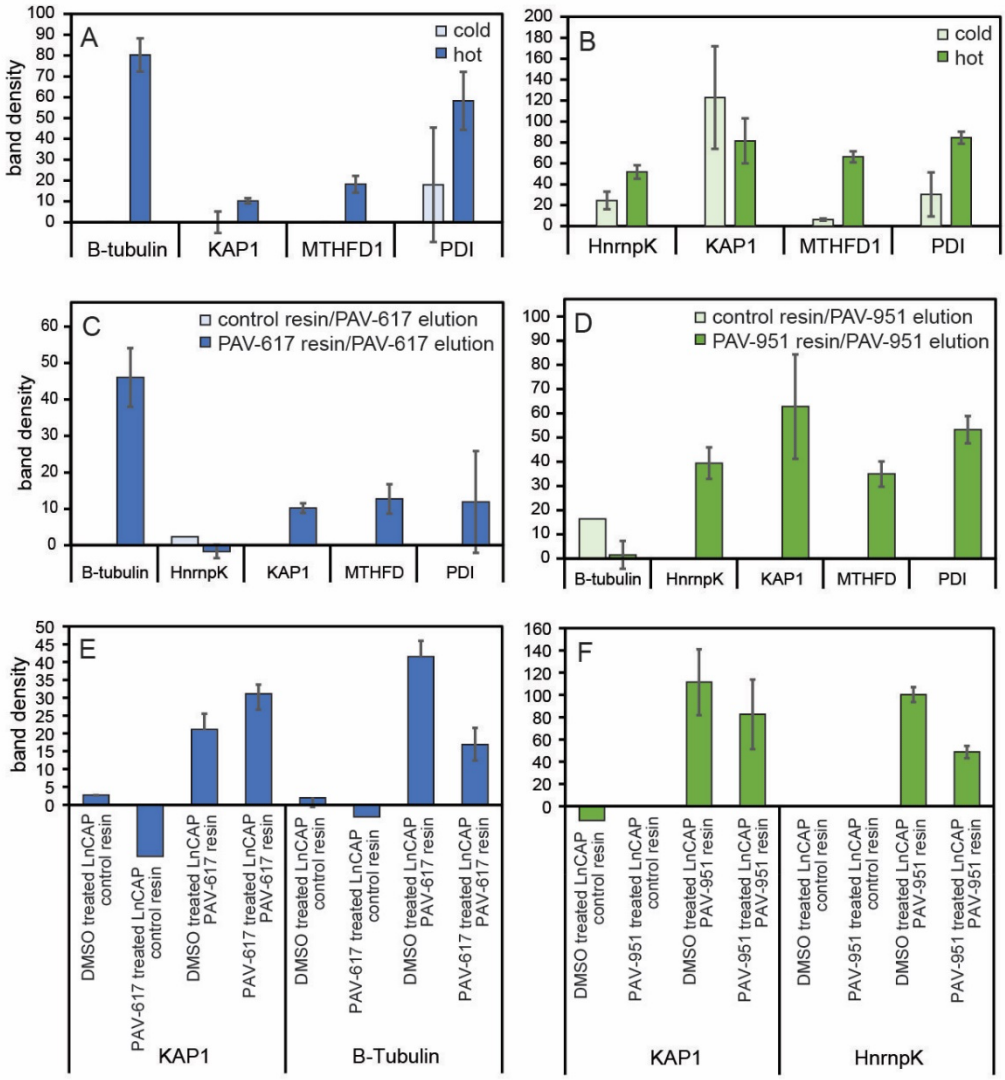

Figure 6. Exploration of changes to PAV-617 and PAV-951 resin eluates under different conditions. DRAC experiments using LnCAP C-33 starting extract as described in **Fig. 5** were conducted under hot conditions which included supplementing the starting material and eluate with an energy cocktail to a final concentration of 1mM rATP, 1mM rGTP, 1mM rCTP, 1mM rUTP, and 0.05 ug/mL creatine kinase and running the experiment at room temperature verus cold conditions at 4 degrees Celsius and without the energy cocktail. **Figs. 6A** and **Fig. 6B** show quantitation of average integrated density of protein band detected by western blot in triplicate-repeat samples eluted with PAV-617 from the PAV-617 or eluted with PAV-951 from the PAV-951 resin when DRAC was conducted side-by-side in hot and cold conditions.

382 **Figs. 6C** and **6D** show quantitation of average integrated density of protein band detected by western blot
383 for TUBB, hnRNPK, KAP1, MTHFD1, and PDI in triplicate-repeat eluates under hot conditions from the
384 PAV-617 resin or PAV-951 resin and a single point elution with each compound from the control resin.
385 Resins were eluted with either compound or 1% DMSO and the amount of protein detected in the 1%
386 DMSO elution is subtracted from the compound elution in the figure. **Fig. 6E** shows quantitation of
387 average integrated density of protein band detected by western blot for KAP1 and B-tubulin in DRAC
388 eluates generated under hot conditions of DMSO versus PAV-617 treated cells eluted with PAV-617 in
389 triplicate from the PAV-617 resin and in single-point from the control resin. **Fig. 6F** shows quantitation of
390 average integrated density of protein band detected by western blot for KAP1 and hnRNPK in DRAC
391 eluates generated under hot conditions for DMSO versus PAV-951 treated cells eluted with PAV-951 in
392 triplicate from the PAV-951 resin or in single-point from the control resin**.**

393

394 One explanation for why the DRAC eluates contain large numbers of proteins is that drug targets
395 for PAV-617 and PAV-951 are themselves multi-protein complexes. To test this hypothesis and
396 determine which proteins directly bind the compounds and which are indirectly associated with the
397 compounds via protein-protein interactions involving the direct drug-binding protein(s), we modified
398 the drug into photocrosslinker analogs by attachment of diazirine and biotin functional groups at the
399 same position to the resin had previously been attached. The photocrosslinker analogs were designed so
400 that after an incubation with cell extract that would allow the compound to bind its target, exposure to
401 ultraviolet light would form a covalent bond between the diazirine moiety of the compound and the
402 nearest protein neighbor (MacKinnon and Taunton, 2009). The sample could then be solubilized and
403 precipitated with streptavidin beads (which bind biotin) to identify the drug-binding protein(s). The
404 streptavidin precipitation (SAP) could be done using a native sample, which would pick up the direct
405 drug-binding proteins(s) and with it any co-associated proteins. Or, the SAP could be done using a

406 denatured sample which would, by virtue of the covalent bond to biotin, identify only the drug-binding
407 protein(s), with all other associated proteins of the target multi-protein complex lost upon denaturation.

408 A549 cell extract was incubated with either 1% DMSO or the photocrosslinker analogs of PAV-
409 617 or PAV-951, then exposed to ultraviolet light. The samples were then divided in two equal parts,
410 where one part was left native and the other denatured, then both were adjusted to non-denaturing
411 conditions and incubated with streptavidin beads. Blots of the SAP samples for KAP1 indicate KAP1 is
412 only a component of the PAV-617 target under native conditions and is completely lost upon
413 denaturation (see **Figs. 7A** and **7B**). However, KAP1 is present to a significant extent in both native and
414 denatured conditions for the SAP with the PAV-951 crosslinker (see **Figs. 7A** and **7C**). The SAP samples
415 were sent for MS-MS analysis, however high background in the samples with no crosslinker added
416 rendered the data uninformative for definitive binding partner identification (data not shown).

417 Conventional methods of drug discovery typically involve the use of recombinant proteins to
418 measure affinity between a drug and its target (Hughes et al., 2011). However, we were concerned that
419 if protein-protein interactions between the direct drug-binding protein and other proteins comprise an
420 important dimension of PAV-617 and PAV-951's targets, isolated recombinant proteins would not be an
421 appropriate surrogate for the protein-protein interactions occurring *in vivo*. To measure target
422 engagement for PAV-617 and PAV-951, we returned to DRAC and determined whether passing a cell
423 extract over the PAV-617 or PAV-951 resins would deplete the extracts of bindable target.

424 We applied the flow-through of PAV-617, PAV-951, and control resins to a second copy of these
425 resins and demonstrated that the drug resins deplete the extract of essentially all KAP1 capable of
426 binding to the resins (see **Figs. 7D** and **7E**). Western blot of the resin flow-through showed that a
427 comparable amount of KAP1 was flowing through the PAV-617, PAV-951, and control resins without
428 binding (see **Fig. 7D**). However, when the flow-through that had been depleted on the PAV-951 resin

429 was applied onto a new PAV-951 resin, very little additional KAP1 bound to the second resin. By
430 contrast, application of the control resin flow-through (which was not specifically depleted of anything)
431 to a second PAV-951 resin, showed significant KAP1 binding to the second resin (see **Fig. 7E**). Application
432 of the PAV-617 resin flow-through to the PAV-951 resin showed significantly more KAP1 binding to the
433 second resin than from the PAV-951 flow-through, but significantly less KAP1 binding than from the
434 control flow-through (see **Fig. 7E**).

435 One notable observation was that, even though the five-fold depletion by PAV-951 resin of its
436 target compared to the control resin was statistically significant and reproducible, it accounted for a tiny
437 amount of the total KAP1 which had been detected by western blot in the starting extract. Only 0.7% of
438 the total amount of KAP1 detected in the starting material bound to the PAV-951 resin after passing
439 over a control column (see **Fig. 7E**). As a reference point to account for non-specific loss of material over
440 the course of the experiment (due to denaturation over time or nonspecific sticking removed during the
441 washing phase)— of the original PAV-951 resin that the extract was depleted with, serial elution with
442 PAV-951 and 1% SDS showed approximately 4% of the total KAP1 detected in the original extract had
443 bound to the resin (data not shown). We conclude that the compounds selectively target this small
444 fraction of KAP1 (less than 5% of the total KAP1 in the extract) because once the subfraction of KAP1
445 capable of binding to the resins is removed, the remaining extract will not bind anymore, even though it
446 still contains ample KAP1.

447 Several of the proteins found by MS-MS in the PAV-617 and PAV-951 resin eluates are known to
448 interact directly with KAP-1 (see **Figs. 7F** and **7G**). These KAP1 implicated proteins include some whose
449 relative amount in the eluate increased and/or decreased with drug treatment and are part of cancer
450 associated interactomes identified from the literature (see **Figs. 7F** and **7G**). The KAP1 implicated
451 proteins from the PAV-951 resin/eluate also contained several proteins that are associated with HIV in

452 the literature (see **Fig. 7G**). These associations may shed light on the cellular role played by the

453 subfractions of KAP1 that are targeted by PAV-617 and PAV-951.

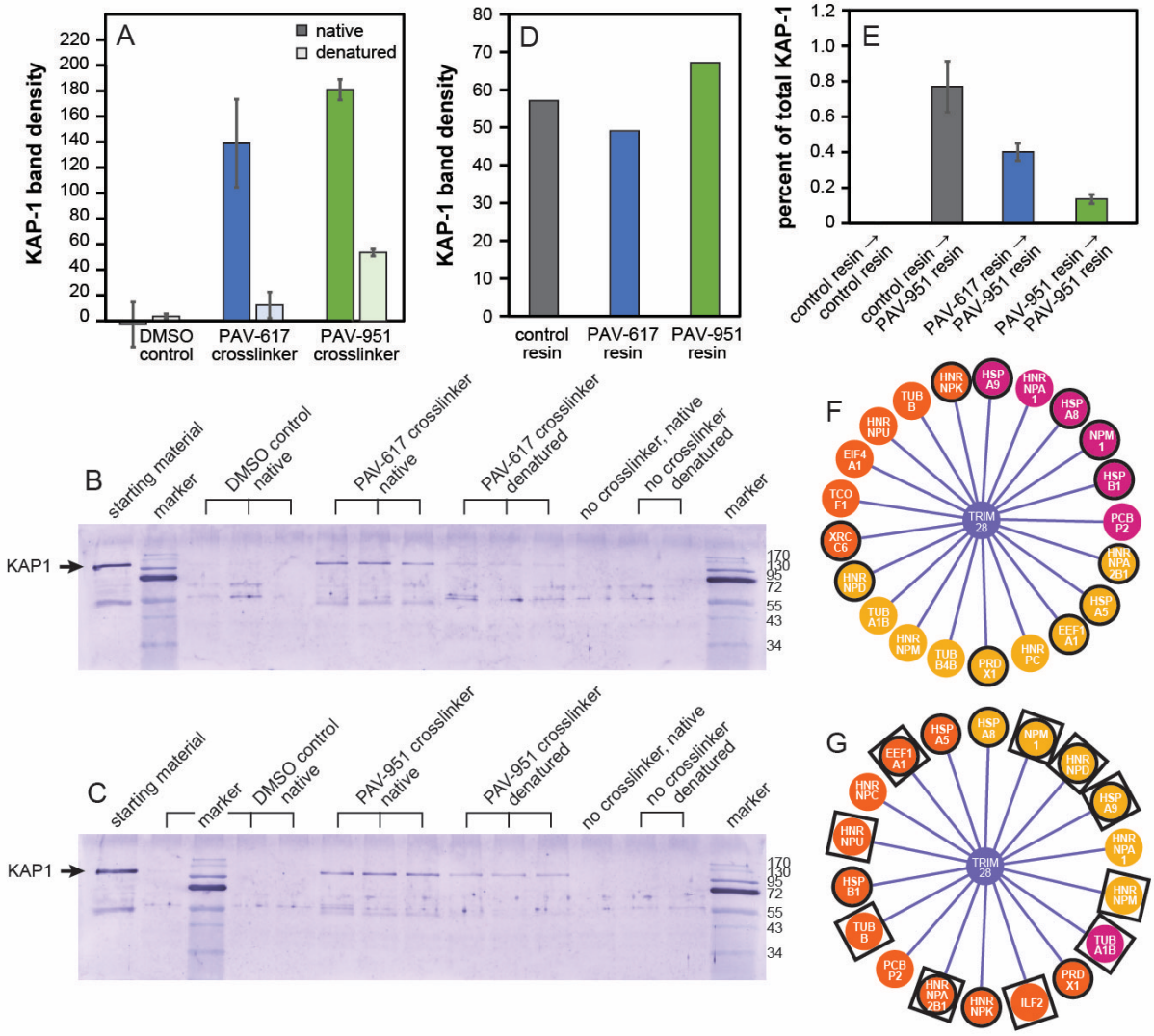

454

455 **Figure 7. KAP-1/TRIM28 as a component of the PAV-617 and PAV-951 target complexes. Fig. 7A** shows

456 quantitation of average integrated density of KAP1 protein band detected by western blot while **Figs. 7B**

457 and **7C** show the western blots themselves, in triplicate-run native and denatured streptavidin

458 precipitations of photo crosslinked samples. Crosslinking experiments were performed where 65 uL of

459 A549 cell extract was adjusted to a protein concentration of approximately 1 mg/ml in column buffer and

460 supplemented with the energy cocktail, with either 1% DMSO or 1uM modified photo crosslinker analogs

461 of PAV-617 and PAV-951 for one hour at room temperature then 20 minutes on ice. The extracts were
462 exposed to UV light then divided into two aliquots. One aliquot was left native and one was denatured by
463 adding DTT, SDS, and boiling. 800 uL of column buffer with 0.1% triton was added to both aliquots and
464 then they were incubated with 2.5ul magnetic streptavidin beads for one hour at room temperature
465 before being denatured in loading buffer containing SDS and heated to 100°C for 3 minutes. **Figs. 7D** and
466 **7E** show the show quantitation of integrated density of KAP1 protein band detected by western blot in
467 LNCaP extract depleted on the PAV-617, PAV-951, and control resins. 230 uL of LNCaP extract was
468 incubated with 230uL of PAV-617, PAV-951, or control resins in single point for one hour in hot conditions.
469 Depleted flow-throughs were divided and put onto a subsequent PAV-951 column in triplicate or onto a
470 subsequent control column in single-point under hot conditions. Columns were eluted three times- a first
471 overnight elution with PAV-951, a second overnight elution with PAV-951, and a third elution with 1%
472 SDS. Eluates were diluted 3:1 in loading buffer and analyzed by western blot. Every western blot for the
473 eluate included a sample of the original, un-depleted starting LNCaP extract diluted 1:100 in loading
474 buffer. **Fig. 7D** shows quantitation from when the flow-throughs from each columns were blotted for
475 KAP1 to determine how much KAP1 had been depleted from each resin. **Fig. 7E** shows the amount of
476 protein detected in the eluate normalized as percent of their corresponding total sample, where the
477 amount detected by eluate samples were divided by the amount detected in the starting material sample,
478 then multiplied by 0.013 to match the concentrations. The percent detected by western blot from the two
479 overnight elutions and the SDS elutions were added together to determine the total percentage of cellular
480 KAP1 was binding to and eluting from the resins). **Figs. 7F** and **7G** show diagrams of proteins identified by
481 MS-MS in Figs. 5A-5C as comprising the PAV-617 resin/eluate and PAV-951 resin/eluate found in the
482 NURSA database of protein-protein interactions as interacting with KAP1
483 (https://dknet.org/about/NURSA_Archive) (Malovannaya et al., 2011). Red indicates KAP1 implicated
484 proteins detected in the eluate which decreased with treatment. Green indicates KAP1 implicated
485 proteins detected in the eluate which increased with treatment. Yellow shows KAP1 implicated proteins
486 detected in the eluate which were unchanged with drug treatment. Circles indicate proteins from the
487 PAV-617 and PAV-951 resin eluates implicated in cancer from the Bushman lab oncogene database

488 (http://www.bushmanlab.org/links/genelists). Squares indicate proteins from the PAV-951 resin
489 eluates implicated in HIV from the virus mentha database (https://virusmentha.uniroma2.it/).

490

491 **Discussion**

492 Our data indicate that PAV-617 and PAV-951, two assembly modulator anti-viral compounds
493 selected for their ability to arrest proliferation in a distinctive way by a novel screen, are cytotoxic to a
494 wide range of neoplastic cell lines representing both rare and common cancers. These compounds,
495 while early in their drug optimization, performed comparably to the commercial anti-cancer drug
496 Gemcitabine, at 10 and 60 fold lower doses, to inhibit the growth of an A549 tumor in immunodeficient
497 mice. These data suggest that these compounds are directed to two different targets common to a wide
498 range of cancers, and may provide a starting point for the development of novel cancer therapeutics.

499 DRAC and photocrosslinking experiments indicate that PAV-617 and PAV-951 interact with
500 proteins that are part of multi-protein complexes. These complexes are dynamic, as demonstrated by
501 changes in the eluate when DRAC is carried out in the presence versus absence of metabolic energy
502 substrates or from untreated versus compound-treated cell starting extract. Together, these findings
503 suggest a model for disease pathogenesis in which previously unappreciated transient multi-protein
504 complexes plays an important role in the dynamics linking cellular proliferation to apoptosis. We
505 hypothesize that cancer progression is facilitated by aberrant versions of these multi-protein complexes
506 and the effect of assembly modulating drugs is to restore the original version of the multi-protein
507 complex, possibly through an allosteric mechanism-of-action (Motlagh and Hisler, 2012), see **Fig. 8**.

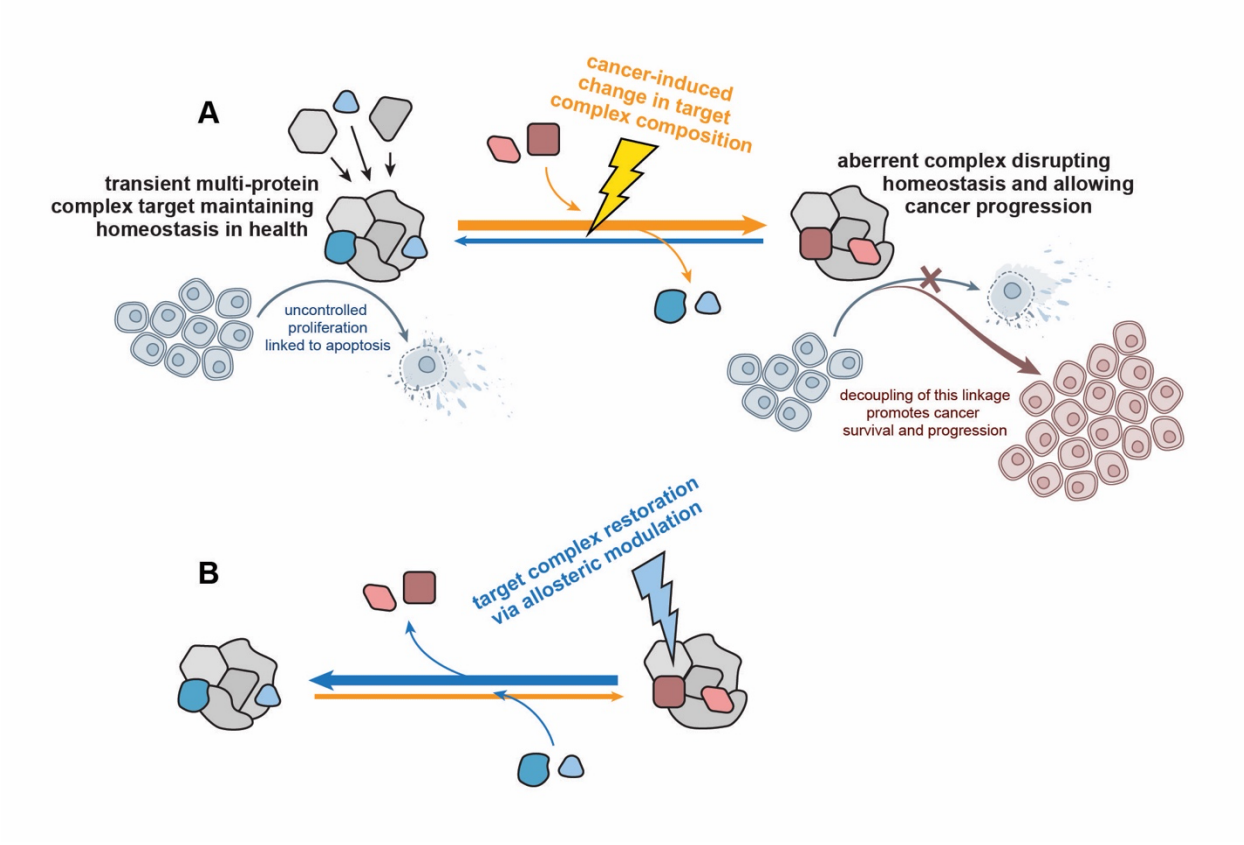

Figure 8. **Cartoon diagram of proposed mechanism of action of assembly modulating compounds**. **Fig. 8A** shows the proposed model where a normal multi-protein complex that plays a role mediating the linkage between uncontrolled proliferation and apoptosis is modified into an aberrant multi-protein complex at a precancerous stage allowing cancer progression rather than homeostatic elimination. **Fig. 8B** shows the proposed mechanism where treatment with an assembly modulating compound restores the original multi-protein complex and its homeostatic functions including elimination of the cancer. Allosteric modulation is indicated as a means by which these changes may be induced.

KAP1/TRIM28, one identified protein component of the PAV-617 and PAV-951 target complexes, is worthy of specific mention. KAP-1 was identified by both MS-MS and western blot as being part of the PAV-617 and PAV-951 targets (see **Figs. 5**, **6**, and **7**). Crosslinking experiments showed that for PAV-617 KAP1 is present in a complex targeted by the compound under native conditions but is lost upon

521 denaturation, indicating it is not a direct drug-binding protein, but rather more likely a distal component
522 of the target multi-protein complex (see **Fig. 7**). For PAV-951, KAP1 is also part of the complex under
523 native conditions and the data indicates a portion of KAP1 may be directly bound to the compound as
524 well. This suggests more than one copy of KAP1 per multi-protein complex (see **Fig. 7**).

525 KAP1 stood out as being of particular interest because it is a known allosteric modulator,
526 implicated in both infectious and noninfectious disease (Randolph et al., 2022, p. 1). KAP1 is involved in
527 a variety of protein-protein interactions and an array of functions including transcriptional activation of
528 HIV, T-cell development, DNA damage repair, as a transcriptional co-repressor for many genes, and as a
529 ligase for post translational modifications such as ubiquitination and SUMOlyation (Iyengar and
530 Farnham, 2011; Randolph et al., 2022). Studies have shown increased levels of KAP-1 in many types of
531 cancer and high levels of KAP-1 correlate with aggressive clinical phenotype and progression to
532 metastasis (Addison et al., 2015; Cui et al., 2014; Yu et al., 2014). However, other described functions of
533 KAP-1 are tumor suppressive and promote autophagy (Neo et al., 2015; Randolph et al., 2022; Yang et
534 al., 2013). KAP-1 directly binds with cancer-implicated proteins including MDM2, TRIM24, Fructose-1,6-
535 biphosphatase (FBP1), MAGE-A3, MAGE-C2, Heat shock protein 70, and TWIST1 (Fong et al., 2018; Jin et
536 al., 2017; Wang et al., 2005; Wei et al., 2016; Yang et al., 2013). The diversity of functions that KAP-1
537 displays appears to be, at least in part, through its assembly into different multi-protein complexes that
538 carry out different objectives.

539 The literature describes that KAP1 is utilized by HIV to the host's detriment but also functions as
540 a key component of the host's immune response in repressing HIV (Allouch et al., 2011; Randolph et al.,
541 2022). KAP1 is implicated as a key part of a pathway hijacked by the poxvirus p28 virulence factor
542 (Huang et al., 2004). We show that PAV-951 is active against HIV and PAV-617 is active against MPXV in
543 addition to their anti-cancer phenotypes. We hypothesize that there are shared alterations in protein
544 assembly in neoplastic cells and virus-infected cells. Advancing the SAR of PAV-617 and PAV-951 could

545 be utilized to determine whether the antiviral and anti-cancer targets are identical or merely similar. In
546 the latter case, the activities would separate with further SAR. Regardless, these findings suggest that
547 the initial CFPSA capsid assembly screen was successful in identifying novel targets relevant to both
548 viruses and cancer.

549 We suggest that PAV-617 and PAV-951 redirect protein-protein interactions, whereby particular
550 proteins are recruited to, and other particular proteins are expelled from, particular multi-protein
551 complexes in the presence of compound. KAP1 is known to both promote and suppress tumorigenesis
552 (Randolph et al., 2022). Therefore, a compound which selectively targets some forms of KAP1 and not
553 others would be important regardless of the nature of the interaction with KAP1. In some cases, as
554 observed for PAV-951, a portion of KAP1 is a direct drug-binding protein, although other copies of KAP1
555 appear not to be. In the case of PAV-617 resin KAP1 is associated with the drug only indirectly by virtue
556 of being a protein present in the target multi-protein complex, but at a distance from the drug-binding
557 site, thus present by SAP under native but not denatured conditions.

558 We interpret the DRAC flow-through data to mean that, by virtue of conformation or other
559 differences among co-associated proteins in a transient multi-protein complex, subfractions of cellular
560 KAP1 are selectively targeted by PAV-617 and PAV-951. Results from the cross-depletion where the
561 flow-through of the PAV-617 resin was applied to a new PAV-951 resin further indicate that the PAV-
562 617-binding subfraction of KAP1 must be distinguishable from the PAV-951-binding subfraction of KAP1
563 because depletion of one does not fully deplete the other (see **Fig. 7E**).

564 These findings about PAV-617 and PAV-951 mirror those made for PAV-104, a structurally
565 unrelated assembly modulator with pan-respiratory anti-viral activity (Müller-Schiffmann et al., 2022). It
566 appears as though assembly modulating compounds, despite structural diversity, share characteristics
567 including the targeting of multi-protein complexes, selectivity for a small fraction of the total amount of

568 a given protein found in a cell, and allosteric mechanisms of action (U. F. Lingappa et al., 2013; Müller-
569 Schiffmann et al., 2022, 2021b; Motlagh and Hisler, 2012). Furthermore, they appear to have
570 remarkable activity across broader categories of pathogens (e.g. pan-viral family and pan-cancer) than is
571 generally observed for existing drugs. The antiviral assembly modulators appear to have a barrier to the
572 development of resistance (Müller-Schiffmann et al., 2022). Further studies are needed to determine
573 whether this property holds true for the anti-cancer subset of assembly modulators.

574 Effective cancer drugs have been developed based on a number of mechanisms including
575 alkylating agents, antimetabolites, antimitotics, and monoclonal antibodies (Falzone et al., 2018).
576 However, as far as we know, no one has attempted to treat cancer through modulation of protein
577 assembly, giving our work with PAV-617 and PAV-951 the potential to be both risky and rewarding.
578 While the animal toxicity of PAV-617 and PAV-951 is higher than would be ideal for the clinic, their anti-
579 tumor activity is already on par with existing cancer drugs and a handful of FDA approved cancer drugs
580 have comparable toxicity gauged by mouse MTD— Cisplatin has a MTD of 6 mg/kg, Doxorubicin has a
581 MTD of 10 mg/kg, and Vinorelbine has a MTD of 10 mg/kg— and many other cancer drugs are
582 administered to patients despite adverse effects because of the urgency of their condition (Aston et al.,
583 2017; Singh and Singh, 2018). Since PAV-617 and PAV-951 are early compounds, further optimization
584 will likely yield chemical analogs with substantially reduced toxicity and further increased activity. We
585 hypothesize that driving SAR toward compounds that are selective for modulating the cancer-induced
586 protein assemblies will improve the therapeutic indexes.

587 Molecular genetic tools such as CRISPR, siRNA knock down, and even use of recombinant
588 protein for protein-protein interaction studies, are unable to parse out the post-translational
589 heterogeneity introduced into proteins as part of normal and aberrant biochemical pathways. The
590 methods applied here are able to do so, as evidenced by the small fraction of the total of specific
591 proteins such as KAP1 found in the target multi-protein complex. It is perhaps not surprising that new

592 tools, and the new targets they allow to be detected, make possible a path to the development of drugs
593 with new properties. Further work will clarify whether, as we hypothesize, the transience of our targets
594 reflects their involvement as a molecular basis for homeostasis. This conclusion, supported by the
595 consequences of assembly modulator treatment both here for cancer and previously for viruses, frames
596 future experiments to better understand this novel approach to more physiological disease
597 therapeutics.

598

599

600

601

602

603

604

605

606

607

608

609

610

611

612

613 **Supplemental Figures**

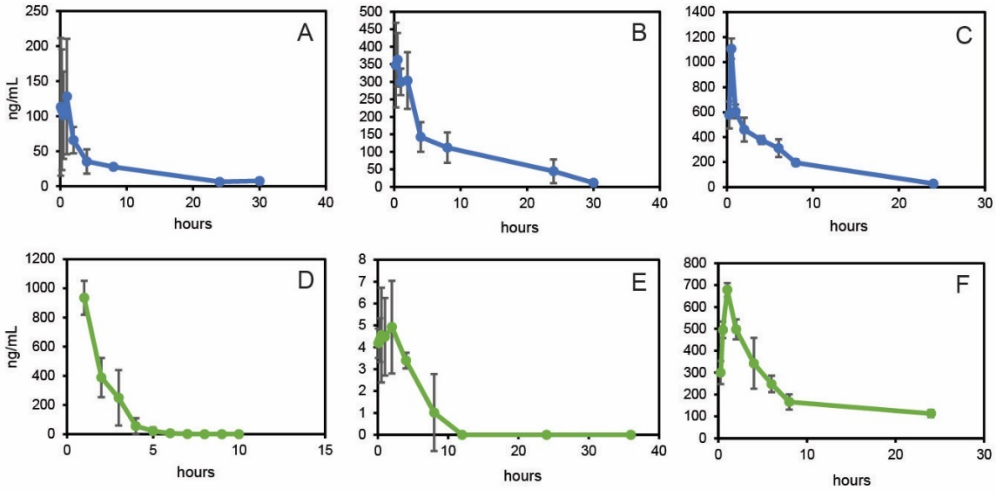

G

animal	route	dose (mg/kg)	C_{max} (uM)	half life (h)	mean residence time (h)
rat	IV	1	2.78	7.84	7.03
rat	IP	5	0.01	7.04	8.31
mouse	oral	10	2.02	5.56	7.66

H

animal	route	dose (mg/kg)	C_{max} (uM)	half life (h)	mean residence time (h)
rat	IV	0.5	0.25	1.68	0.63
rat	IP	2.5	0.71	nd	2.92
mouse	oral	10	2.16	13.6	19.3

614

615

616 **Supplemental Figure 1. Summary of PAV-617 and PAV-951 PK properties. Supplemental Figs. A-F** show
617 plasma concentration over time for PAV-617 and PAV-951 when given to animals via three different
618 routes of administration. Randomized treatment groups of four male Sprague Dawley rats or three CD1
619 mice were administered vehicle, PAV-617, or PAV-951 either IV, IP, or orally and blood samples were
620 collected before injection as well as at different time points after dosing. The concentration of compound
621 in the plasma at different time points was measured by LC MS/MS. **Supplemental Fig. G** summarizes PK
622 properties observed for PAV-617 based on animal, administration route, and dose. **Supplemental Fig. H**
623 summarizes the PK properties observed for PAV-951 based on animal, administration route, and dose.
624 The maximum concentration (Cmax) was determined to be the highest measured concentration within a

625 dataset. The half life was calculated as time required for the concentration of compound in the animal's
626 plasma to decrease by half. The mean residence time was calculated as the average time the compound
627 remained in the animal.

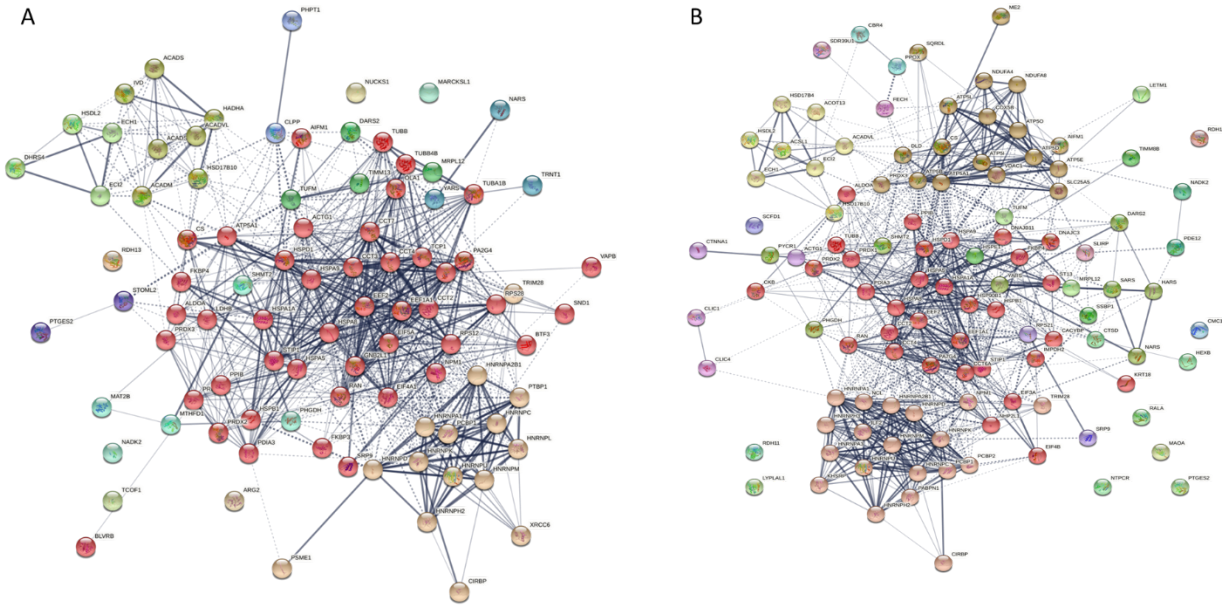

628

629 **Supplemental Figure 2. Known protein-protein interactions among PAV-617 and PAV-951 eluate**
630 **components**. **Supplemental Fig. 2A** and **2B** show string-diagram analyses of the protein-protein
631 interaction network of proteins identified in **Figs. 5A-5C** by tandem MSMS as comprising the PAV-617
632 (**Supplemental Fig. 2A)** and PAV-951 (**Supplemental Fig. 2B**) targets. Proteins were entered into the string
633 database (string-db.org). The confidence mode view is shown where the confidence level was set to 0.4
634 (medium) and MCL clustering was applied with the inflation parameter of 3. The dotted lines represent
635 edges between different clusters. The thickness of the lines represent the degree of confidence for each
636 protein-protein interaction.

637

638

639

640 **Materials and Methods**

641 **Lead Contact and Materials Availability**

642 Further information and requests for resources and reagents should be directed to and will be fulfilled
643 by the Lead Contact Vishwanath Lingappa (vlingappa@prosetta.com).

644 Use of unique compounds PAV-617 and PAV-951 and their stable derivatives may be available upon
645 request by the Lead Contact if sought for experimental purposes under a valid completed Materials
646 Transfer Agreement.

647 The number of replicates carried out for each experiment is described in the figure/table legends.

648

649 **Experimental Models and Subject Details**

650 **Animal models**

651 Maximum tolerated dose (MTD) studies were conducted using female Balb/C mice, aged 8-10
652 weeks or female CD1 mice, aged 5-6 weeks. Treatment groups were made up of 3 animals each, unless
653 otherwise noted, and dosing regimens for disclosed data is provided. Animals were sacrificed at the end
654 of the study period using an overdose of CO2. MTD studies were conducted at Vipragen Biosciences
655 Private Limited in accordance with the Committee for the Purpose of Control and Supervision of
656 Experiments on Animals (CPCSEA) guidelines and Animal Research: Reporting of In Vivo Experiments
657 (ARRIVE) guidelines.

658 Pharmacokinetic (PK) studies were conducted in male Sprague Dawley Rats aged 8-10 weeks or
659 male CD1 mice aged 5-6 weeks. Treatment groups were made up of 4 animals each and dosing regimens
660 for disclosed data is provided. Animals were sacrificed at the end of the study period using an overdose

661 of CO2. PK studies were conducted at Vipragen Biosciences Private Limited in accordance with the
662 Committee for the Purpose of Control and Supervision of Experiments on Animals (CPCSEA) guidelines
663 and Animal Research: Reporting of In Vivo Experiments (ARRIVE) guidelines.

664 Tumor xenograft studies were conducted using female Athymic Nude mice, strain CrTac: Ncr-
665 Foxn1^{nu}, aged 6-8 weeks. Tumor transplantation occurred through subcutaneous injection of a 0.1mL
666 cell suspension containing 1 to 5x10^{6} A549 lung cancer cells obtained from ATCC in Matrigel in PBS into
667 the left flank region of the mice. Treatment groups were made up of 6 animals each and dosing
668 regimens for disclosed data is provided. Animals were sacrificed at the end of the study period using an
669 overdose of isoflurane anesthesia. Both xenograft studies were conducted at Anthem Biosciences
670 Private Limited in Bangalore, India and were approved by the Institutional Animal Ethics committee
671 (IAEC) of Anthem Biosciences in accordance with the Committee for the Purpose of Control and
672 Supervision of Experiments on Animals (CPCSEA) guidelines and Animal Research: Reporting of *In Vivo*
673 Experiments (ARRIVE) guidelines.

674

675 **Cell lines**

676 The *in vivo* xenograft study utilized the A549 (male human lung cancer). Cells were grown under
677 sterile conditions. These studies were conducted at Anthem Biosciences Private Limited in Bangalore,
678 India.

679 The Human tumor cell proliferation assay used A172 (male human glioma), BFTC-905 (female
680 human urinary bladder transitional cell carcinoma), COR-L105 (male human lung adenocarcinoma), DB
681 (male human b-cell lymphoma), FaDu (male human pharynx squamous cell carcinoma), H9 (male human
682 t-cell lymphoma), Hs 294T (male human melanoma), MCF7 (female human breast cancer), MDA MB 436
683 (female human breast cancer), MeWo (male human melanoma), MHH-PREB-1 (male human b-cell

684 lymphoma), SJSA1-OSA (male human osteosarcoma), SU-DHL-10 (male human b-cell lymphoma),
685 SW1353 (female human chondrosarcoma), and U-2 OS (female human osteosarcoma) cell lines. This
686 study was conducted by Eurofins Scientific as part of their OncoPanel™.

687 The monkey pox virus infectious virus assay used BSC-40 cells (nonhuman primate kidney) and
688 MPXV Zaire 79 strain. These studies were conducted by the United States Army Medical Research
689 Institute of Infectious Diseases on Fort Detrick, Maryland.

690 Human immunodeficiency virus infectious virus assay used MT-2 cells (female human t-cell
691 leukemia) and the NL4-3 Rluc reporter virus. These studies were conducted at the University of
692 Washington in Seattle, Washington.

693 The *in vitro* screens for apoptosis, high-density/ low-density activity, and cell growth recovery
694 utilized the LNCaP C-33 (male human prostate cancer), LNCaP C-81 (male human prostate cancer), CHO-
695 K1 (Chinese Hamster ovary), and Hennes 20 (Chinese Hamster ovary) cell lines. Cells were grown under
696 sterile conditions. These studies were conducted at Prosetta Biosciences in San Francisco, California.

697 The *in vitro* drug resin affinity chromatography and photocrosslinking experiments utilized A549
698 (male human lung cancer) or LNCaP C-33 (male human prostate cancer) cell line. Cells were grown under
699 sterile conditions. Sterile conditions were not maintained once cells were harvested for *in vitro*
700 experiments. These studies were conducted at Prosetta Biosciences in San Francisco, California.

701 ***In vitro* experiments**

702 Drug resin affinity chromatography and photocrosslinking experiments, and SDS-PAGE/Western
703 Blot analysis of the results, were conducted by Prosetta Biosciences in San Francisco, California under
704 conditions described in figure legends. Results from disclosed *in vitro* experiments were repeated in

705 triplicate unless otherwise stated. Mass spectrometry analysis of samples were conducted by MS
706 Bioworks in Ann Arbor, Michigan.

707 **Method and Analysis Details**

708 **Monkey pox infectious virus assay**

709 BSC-40 cells of 95% confluence in 24-well plates were infected with100 pfu of MPXV Zaire 79
710 diluted in Eagle's Minimum Essential Medium with 2% fetal bovine serum and incubated in 37 degrees
711 Celsius in 5% CO_2 for 1 hour. The viral inocula were removed and replaced with the test compounds in
712 six half log dilutions (0.1 ml per well) and the cells were overlaid with 1% methylcellulose in growth
713 media (1 ml per well). The media and virus control cells received growth medium containing 1%
714 methylcellulose. After three days of infection, when plaques appeared, cells were stained with crystal
715 violet for an hour and then washed with water and dried overnight. The plaques were counted the next
716 day and virus-only wells were compared with the compound-added wells to determine percentage
717 protection. Infected cells were stained with crystal violet and viral plaques were counted. Averages and
718 standard deviation for plaques observed under different treatment conditions were calculated in
719 Microsoft Excel and graphed as the percent inhibition in PAV-617 treated cells compared to untreated
720 cells.

721

722 **Human immunodeficiency virus infectious virus assay**

723 MT-2 cells were preseeded in 96-well plates in 100 ul of complete RPMI. Multiple
724 concentrations of PAV-951 were serially diluted in DMSO then into an infection media prepared by
725 diluting NL4-3 Rluc virus stock to 400 IU/100 ul with complete RPMI, which was transferred onto the
726 MT-2 cells with a final MOI of 0.02 and final DMSO concentration of 1% in infected places. One well

727 received DMSO only, instead of PAV-951, and one well received medium only for normalization and
728 background collection. Cells were incubated at 37 degrees Celsius for 96 hours. 100ul of medium was
729 removed and discarded and 10 ul of 15 uM EnduRen luciferase substrate was added to each well,
730 followed by incubation for 1.5 hours at 37 degrees Celsius. Plates were read on a luminescence plate
731 reader. Bioluminescence intensity was read on a Synergy H1 BioTek plate reader. Averages and standard
732 deviation for viral titer observed under different treatment conditions were calculated in Microsoft Excel
733 and graphed as the percent inhibition in PAV-951 treated cells compared to untreated cells.

734

735 **Apoptosis Screen**

736 A 96 well plate was seeded with Hennes 20 cells at 500 cells per well, CHO-K1 cells at 500 cells
737 per well, LNCaP C-33 cells at 2000 cells per well, and LNCaP C-81 cells at 2000 cells per well. Cells were
738 grown in 100uL minimum essential media for three days then three wells of each cell line received
739 treatment with 1% DMSO. 12 hours after drug treatment, a mixture of 25 ul media and 25 ul Apo-ONE
740 reagent (Promega) was added then the plate was covered and placed on a shaker at room temperature
741 for six hours. The plate was read on a microplate reader for fluorescence at 499/521. Values were
742 averaged and standard deviations were calculated for each triplicate condition and graphed on
743 Microsoft Excel.

744

745 **High density/ low density assay**

746 Two 96 well plates were seeded with Hennes 20 cells in parallel where one was plated at a
747 density of 500 cells/well and the other was plated at a density of 15,000 cells/well. 90 ul of minimum
748 essential media was added to each well and plates were placed in a 37 degrees Celsius incubator for 24

749 hours. The next day, 10ul of media containing dilutions of compound in DMSO were added to each plate
750 in triplicate with final concentrations of 0.025 uM PAV-617, 0.05 uM PAV-617, 0.1 uM PAV-617, 0.5 uM
751 PAV-617, 0.02 uM PAV-951, 0.3 uM PAV-951, 0.4 uM PAV-951, or 0.5 uM PAV-951. Six wells on each
752 plate received 10ul of media containing only DMSO. Each well was gently mixed 5 times with a 100ul
753 pipette. Plates were incubated at 37 degrees Celsius for 72 hours then 10 uL of alamarBlue was added to
754 each well. Wells were mixed 5 times then incubated at 37 degrees Celsius for 72 hours. Plates were then
755 read at 530/590. Values were averaged and standard deviations were calculated for each triplicate
756 condition and graphed on Microsoft Excel.

757

758 **Cell growth recovery assay**

759 A 96 well plate was seeded with either Hennes 20 or LNCaP C-33 cells at 500 cells/well in 90 uL
760 of minimum essential media and incubated at 37 degrees Celsius for 24 hours. 0.5% DMSO was diluted
761 in media and added to 6 control wells for each plate. PAV-617 was diluted in media and added to three
762 wells at a concentration of 0.3 uM. PAV-951 was diluted in media and added to concentration of 0.4 uM.
763 After 24 hours of PAV-617 treatment or 6 hours of PAV-951 treatment, the medium containing
764 compound was removed and replaced with fresh media. After 72 hours (day 5), plates were assayed
765 with alamarBlue and fluorescence was read at 530/590. The medium containing alamarBlue was
766 removed and replaced with fresh media. After another 72 hours (day 8) plates were assayed with
767 alamarBlue and fluorescence again, then medium containing alamarBlue was removed and replaced
768 with fresh media. After a final 72 hour incubation (day 11) plates were assayed with alamarBlue one
769 more time. Average fluorescence for each day and treatment condition were plotted on Microsoft Excel
770 with standard deviation calculated to provide error bars.

771

772 **Human tumor cell proliferation assay**

773 A panel of human tumor cell lines (A172, BFTC-905, COR-L105, DB, FaDu, H9, Hs 294T, MCF7,
774 MDA MB 436, MeWo, MHH-PREB-1, SJSA1-OSA, SW1353, and U2OS) were grown in RPMI 1640, 10%
775 FBS, 2 mM L-alanyl-L-glutamine, 1 mM Na pyruvate. Cells were seeded into 384-well plates and
776 incubated in a humidified atmosphere with 5% CO2 at 37C. After 24 hours of incubation DMSO, PAV-
777 617, or PAV-951 was added at concentrations of 5 uM, 1 uM, and 0.2 uM and plates were incubated for
778 3 days. Then cells were lysed with CellTiter-Glo (Promega) which generates a bioluminescence signal
779 relative to ATP levels and is used as a measurement of viable cells. Bioluminescence was read by a
780 PerkinElmer Envision microplate reader. Bioluminescence intensity was measured by a PerkinElmer
781 Envision microplate reader and transformed to a percent of control (POC) using the formula:
782 POC=(Ix/I0)*100, where Ix is the whole well signal intensity at a given treatment, and I0 is the average
783 intensity of the untreated vehicle wells. Values were averaged for each triplicate condition and graphed
784 on Microsoft Excel.

785

786 **Mouse maximum tolerated dose studies**

787 For the intraperitoneal MTD study, female Balb/c mice aged 8-10 weeks were randomly divided
788 into treatment groups with three animals per group. Animals in each treatment group were weighed
789 and received one IP injection of 0.1-0.15mL containing either vehicle (10% DMSO, 45% propylene glycol,
790 45% sterile water), 1mg/kg PAV-617, 2 mg/kg PAV-617, 5 mg/kg PAV-617, 10 mg/kg PAV-617, 1mg/kg
791 PAV-951, 2.5 mg/kg PAV-951, 5mg/kg PAV-951 or 10 mg/kg PAV-951. Animals were observed from day 0
792 until day 3 for clinical signs of toxicity. Animals were euthanized after 72 hours and were examined
793 externally and internally by a pathologist for abnormalities in organ weight and tissue damage. Blood

794 samples were sent for a complete blood count bioanalysis. MTD was determined to be the dose at
795 which no signs of toxicity were observed by any parameters.

796 For the oral MTD study, female CD1 mice aged 5-6 weeks were given either an oral dose of vehicle (10%
797 DMSO, 45% propylene glycol, 45% sterile water) or either 10 mg/kg or 20 mg/kg of PAV-617 or PAV-951.
798 The vehicle and 20 mg/kg groups had three animals each, while the 10 mg/kg groups only had one
799 animal. Animals were observed for clinical signs and after a week they were euthanized and examined
800 externally and internally by a pathologist for changes related to toxicity.

801

802 **Pharmacokinetics studies**

803 For the IP and IV PK studies, male Sprague Dawley rats aged 8-10 weeks were randomly divided
804 into treatment groups with four animals per group. Animals in each treatment group were weighed and
805 received one 2.4 mL intravenous dose of either vehicle (10% DMSO, 45% propylene glycol, 45% sterile
806 water), 1mg/kg PAV-617, or 0.5 mg/kg PAV-951, or one intraperitoneal dose of either vehicle (100%
807 labrasol), 5mg/kg PAV-617 or 2.5 mg/kg PAV-951 . Blood was collected from a pre-cannulated line
808 before dosing, and subsequently 15 minutes, 30 minutes, 1 hour, 2 hours, 4 hours, 8 hours, 12 hours, 24
809 hours, and 30 hours post-dosing. Concentration of drug in the plasma over time was measured using a
810 Waters Acquity TQD LCMS/MS. Maximum concentration (Cmax) was determined to be the maximum
811 concentration detected in a dataset. Half life, area under the curve, and mean residence time were
812 calculated with Phoenix WinNolin software.

813 For the oral PK studies, male CD1 mice aged 5-6 weeks were randomly divided into treatment
814 groups with three animals per group. Animals in each treatment group were weighed and received, via
815 oral gavage needle, either one oral dose of vehicle (10% DMSO, 45% propylene glycol, 45% sterile
816 water), 10 mg/kg PAV-617, or 10 mg/kg PAV-951. Blood was collected from a pre-cannulated line before

817 dosing, and subsequently 2 minutes, 5 minutes, 15 minutes, 30 minutes, 1 hour, 2 hours, 4 hours, 6
818 hours, 8 hours, and 24 hours post-dosing. Concentration of drug in the plasma over time was measured
819 using a Waters Acquity TQD LCMS/MS. Maximum concentration (Cmax) was determined to be the
820 maximum concentration detected in a dataset. Half life, area under the curve, and mean residence time
821 were calculated with Phoenix WinNolin software.

822

823 **Animal xenograft study**

824 A549 cells growing in RPMI-1640 medium were suspended with Matrigel in PBS. 0.1 ml of cell
825 suspension containing 1 x 106 cells were injected subcutaneously into the left flank region of female, 6-8
826 weeks old nude mice (CrTac: Ncr-Foxn1nu). After 30 days of tumor establishment, mice were divided
827 randomly into treatment groups. In the PAV-617 study, 6 animals were treated with vehicle only (10%
828 DMSO, 10% propylene glycol, 80% sterile water) by IP once daily, 6 animals were treated with 100
829 mg/kg Gemcitabine Hydrochloride by IP twice weekly, and 6 animals were treated with 10 mg/kg PAV-
830 617 by IP once daily for 28 days. In the PAV-951 study, 6 animals were treated with vehicle only (10%
831 DMSO, 10% propylene glycol, 80% sterile water) by IV once daily, 6 animals were treated with 100
832 mg/kg Gemcitabine by IV twice weekly, and 6 animals were treated with 1.5 mg/kg PAV-951 by IV once
833 daily for 14 days. In both studies, mice were weighed and their tumors were measured using a digital
834 Vernier caliper. Tumor volume was calculated using the formula: $(L \times W^2)/2$ where L is the largest
835 diameter and W is the smallest diameter of the tumor. Statistical analysis was performed using Graph
836 Pad Prism (Ver. 5.03). Statistical analysis of tumor growth inhibition between the Control and Treated
837 groups was performed by using One-way ANOVA followed by Dunnett's test.

838

839

840 **Drug Resin affinity chromatography**

841 LNCaP C-33 cells were grown in minimum essential media (UCSF) with 10% FBS and 1% Penstrep
842 for 24 hours then treated with 500nM PAV-617, 500nM PAV-951, or DMSO for 22 hours. Cells were
843 scraped into cold phosphate buffered saline (PBS) (10mM sodium phosphate, 150 mM sodium chloride
844 pH 7.4), then spun at 1,000 rpm for 10 minutes until pelleted. The PBS was decanted and the pellet
845 resuspended in a low salt buffer (10mM HEPES pH 7.6, 10mM NaCl, 1mM MgAc with 0.35% Tritonx100)
846 then centrifuged at 10,000 rpm for 10 minutes at 4 degrees Celcius. The post-mitochondrial supernatant
847 was removed and adjusted to a concentration of approximately 10 mg/ml and equilibrated in a
848 physiologic column buffer (50 mM Hepes ph 7.6, 100 mM KAc, 6 mM MgAc, 1 mM EDTA, 4mM TGA). In
849 some conditions, the extract was supplemented with an energy cocktail (to a final concentration of
850 1mM rATP, 1mM rGTP, 1mM rCTP, 1mM rUTP, and 5 ug/mL creatine kinase). 30 ul or 230 ul of extract
851 was then incubated for one hour at either 4 degrees Celcius or 22 degrees Celsius on 30 ul or 230 ul of
852 affigel resin coupled to either PAV-617, PAV-951, or a 4% agarose matrix (control). The input material
853 was collected and the resin was then washed with 3 ml column bufffer. The resins were eluted overnight
854 at either 4 degrees Celcius or at 22 degrees Celsius in 100ul or 330ul column buffer containing either
855 100uM PAV-617 or 100uM PAV-951 or DMSO, with or without the energy cocktail. Eluates were run on
856 western blot or sent for mass spectrometry for analysis.

857

858 **Chemical photocrosslinking**

859 A549 extract was prepared as above then adjusted to a protein concentration of approximately
860 1 mg/ml in column buffer containing 0.01% triton and supplemented with the energy cocktail (to a final
861 concentration of 1mM rATP, 1mM rGTP, 1mM rCTP, 1mM rUTP, and 5 ug/mL creatine kinase).
862 Photocrosslinker analogs of PAV-617 and PAV-951 chemically modified to contain biotin and a diazirine

863 group or 1% DMSO were added to 67 ul of extract at 100uM, incubated for one hour at 22 degrees
864 Celsius followed by 20 minutes on ice, then exposed to ultraviolet light for 5 minutes at 22 degrees
865 Celsius. After crosslinking, samples were divided in two 30 ul aliquots and one set was denatured by
866 adding 5 ul of 10% SDS, 0.625 ul DTT, and boiling for 5 minutes. Both native and denatured aliquots
867 were then diluted in 800 ul column buffer containing 0.1% triton. 2.5 ul of magnetic streptavidin beads
868 (Pierce) were added to all samples and mixed for one hour at room temperature to capture all
869 biotinylated proteins and co-associated proteins. Samples were placed on a magnetic rack to hold the
870 beads in placed and washed three times with 800 ul of column buffer containing 0.1% triton. After
871 washing, beads were resuspended in 80 ul of gel loading buffer containing SDS and analyzed by western
872 blot or blot for affinity purified streptavidin. Samples were analyzed by western blot.

873

874 **Western blotting**

875 SDS/PAGE gels were transferred in Towbin buffer (25mM Tris, 192mM glycine, 20% w/v
876 methanol) to polyvinylidene fluoride membrane, blocked in 1% bovine serum albumin (BSA) in PBS,
877 incubated overnight at 4 degrees Celsius in a 1:1,000 dilution of 100ug/mL affinity-purified primary IGG
878 to KAP-1, MTHFD1, hnRNPk, TUBB, or PDI in 1% BSA in PBS containing 0.1% Tween-20 (PBST).
879 Membranes were then washed twice in PBST and incubated for two hours at room temperature in a
880 1:5000 dilution of secondary anti-rabbit or anti-mouse antibody coupled to alkaline phosphatase in
881 PBST. Membranes were washed two more times in PBST then incubated in a developer solution
882 prepared from 100 uL of 7.5 mg/mL 5-bromo-4-chloro-3-indolyl phosphate dissolved in 60% dimethyl
883 formamide (DMF) in water and 100ul of 15 mg/ml nitro blue tetrazolium dissolved in 70% DMF in water,
884 adjusted to 50mL with 0.1 Tris (pH 9.5) and 0.1 mM magnesium chloride. Membranes were scanned and

885 the integrated density of protein band was measured on ImageJ. Averages and the standard deviation
886 between repeated experiments were calculated and plotted on Microsoft Excel.

887 **Tandem mass spectrometry**

888 Samples were processed by SDS PAGE using a 10% Bis-ttris NuPAGE gel with the MES buffer
889 system. The mobility region was excised and washed with 25 mM ammonium bicarbonate followed by
890 15mM acetonitrile. Samples were reduced with 10 mM dithoithreitol and 60 degrees Celsius followed by
891 alkylation with 5o mM iodacetamide at room temperature. Samples were then digested with trypsin
892 (Promega) overnight (18 hours) at 37 degrees Celcius then quenched with formic acid and desalted using
893 an Empore SD plate. Half of each digested sample was analyzed by LC-MS/MS with a Waters
894 NanoAcquity HPLC system interfaced to a ThermoFisher Q Exactive. Peptides were loaded on a trapping
895 column and eluted over a 75 uM analytical column at 350 nL/min packed with Luna C18 resin
896 (Phenomenex). The mass spectrometer was operated in a data dependent mode, with the Oribtrap
897 operating at 60,000 FWHM and 15,000 FWHM for MS and MS/MS respectively. The fifteen most
898 abundant ions were selected for MS/MS.

899 Data was searched using a local copy of Mascot (Matrix Science) with the following parameters:
900 Enzyme: Trypzin/P; Database: SwissProt Human (concated forward and reverse plus common
901 contaminants); Fixed modification: Carbamidomethyl (C) Variable modifications: Oxidation (M), Acetyl
902 (N-term), Pyro-Glu (N-term Q), Deamidation (N/Q) Mass valuse: Monoisotopic; Peptide Mass Tolerance:
903 10 ppm; Gragment Mass Tolerance: 0.02 Da; Max Missed Cleavages: 2. The data was analyzed by label
904 free quantitation (LFQ) and spectral count methods. LFQ intensity values of each condition were
905 measured in triplicate and compared against each other to generate $\log_2$ fold change values for each
906 combination of conditions. Spectral counts were filtered for a 1% protein/peptide false discovery rate
907 requiring 2 unique peptides per protein and the data set was furher adjusted by substraction of spectral

908 counts for specific proteins observed in the control resin. Identified proteins were spearched in the
909 NURSA database of protein-protein interactions (https://dknet.org/about/NURSA_Archive) to determine if
910 they interact with KAP-1, the Bushman labs oncogene database
911 (http://www.bushmanlab.org/links/genelists) to determine if they were known to be implicated in
912 cancer, and the VirusMentha database (https://virusmentha.uniroma2.it/) to determine if they interact
913 with HIV. String diagrams of protein-protein interaction networks were generated using the STRING
914 database (string-db.org).

915

916

917

918

919 **Acknowledgements:**

920 We thank Usha F. Lingappa for help with the figures, Dmitry Temnikov for IT support, Halley McCormick
921 for help with data analysis, and Jairam R. Lingappa for valuable suggestions during manuscript
922 preparation.

923

924 **Competing interests:**

925 Vishwanath R. Lingappa is CEO of Prosetta Biosciences.

926

927 **References**

928 Addison, J.B., Koontz, C., Fugett, J.H., Creighton, C.J., Chen, D., Farrugia, M.K., Padon, R.R., Voronkova,
929 M.A., McLaughlin, S.L., Livengood, R.H., Lin, C.-C., Ruppert, J.M., Pugacheva, E.N., Ivanov, A.V.,
930 2015. KAP1 Promotes Proliferation and Metastatic Progression of Breast Cancer Cells. Cancer
931 Res. 75, 344–355. https://doi.org/10.1158/0008-5472.CAN-14-1561
932 Allouch, A., Di Primio, C., Alpi, E., Lusic, M., Arosio, D., Giacca, M., Cereseto, A., 2011. The TRIM Family
933 Protein KAP1 Inhibits HIV-1 Integration. Cell Host Microbe 9, 484–495.
934 https://doi.org/10.1016/j.chom.2011.05.004
935 Aston, W.J., Hope, D.E., Nowak, A.K., Robinson, B.W., Lake, R.A., Lesterhuis, W.J., 2017. A systematic
936 investigation of the maximum tolerated dose of cytotoxic chemotherapy with and without
937 supportive care in mice. BMC Cancer 17, 684. https://doi.org/10.1186/s12885-017-3677-7
938 Broce, S., Hensley, L., Sato, T., Lehrer-Graiwer, J., Essrich, C., Edwards, K.J., Pajda, J., Davis, C.J.,
939 Bhadresh, R., Hurt, C.R., Freeman, B., Lingappa, V.R., Kelleher, C.A., Karpuj, M.V., 2016.
940 Biochemical and biophysical characterization of cell-free synthesized Rift Valley fever virus
941 nucleoprotein capsids enables in vitro screening to identify novel antivirals. Biol. Direct 11, 25.
942 https://doi.org/10.1186/s13062-016-0126-5
943 Cirone, M., 2018. EBV and KSHV Infection Dysregulates Autophagy to Optimize Viral Replication, Prevent
944 Immune Recognition and Promote Tumorigenesis. Viruses 10, 599.
945 https://doi.org/10.3390/v10110599
946 Copley, S.D., 2012. Moonlighting is mainstream: Paradigm adjustment required. BioEssays 34, 578–588.
947 https://doi.org/10.1002/bies.201100191
948 Cui, Y., Yang, S., Fu, X., Feng, J., Xu, S., Ying, G., 2014. High Levels of KAP1 Expression Are Associated with
949 Aggressive Clinical Features in Ovarian Cancer. Int. J. Mol. Sci. 16, 363–377.
950 https://doi.org/10.3390/ijms16010363

951 Falzone, L., Salomone, S., Libra, M., 2018. Evolution of Cancer Pharmacological Treatments at the Turn
952 of the Third Millennium. Front. Pharmacol. 9, 1300. https://doi.org/10.3389/fphar.2018.01300
953 Fong, K., Zhao, J.C., Song, B., Zheng, B., Yu, J., 2018. TRIM28 protects TRIM24 from SPOP-mediated
954 degradation and promotes prostate cancer progression. Nat. Commun. 9, 5007.
955 https://doi.org/10.1038/s41467-018-07475-5
956 Gad, S.C., 2014. Maximum Tolerated Dose, in: Encyclopedia of Toxicology. Elsevier, p. 164.
957 https://doi.org/10.1016/B978-0-12-386454-3.00874-5
958 Hanahan, D., Weinberg, R.A., 2011. Hallmarks of Cancer: The Next Generation. Cell 144, 646–674.
959 https://doi.org/10.1016/j.cell.2011.02.013
960 Hanahan, D., Weinberg, R.A., 2000. The Hallmarks of Cancer. Cell 100, 57–70.
961 https://doi.org/10.1016/S0092-8674(00)81683-9
962 Huang, J., Huang, Q., Zhou, X., Shen, M.M., Yen, A., Yu, S.X., Dong, G., Qu, K., Huang, P., Anderson, E.M.,
963 Daniel-Issakani, S., Buller, R.M.L., Payan, D.G., Lu, H.H., 2004. The Poxvirus p28 Virulence Factor
964 Is an E3 Ubiquitin Ligase. J. Biol. Chem. 279, 54110–54116.
965 https://doi.org/10.1074/jbc.M410583200
966 Hughes, J., Rees, S., Kalindjian, S., Philpott, K., 2011. Principles of early drug discovery: Principles of early
967 drug discovery. Br. J. Pharmacol. 162, 1239–1249. https://doi.org/10.1111/j.1476-
968 5381.2010.01127.x
969 Igawa, T., Lin, F.-F., Lee, M.-S., Karan, D., Batra, S.K., Lin, M.-F., 2002. Establishment and characterization
970 of androgen-independent human prostate cancer LNCaP cell model. The Prostate 50, 222–235.
971 https://doi.org/10.1002/pros.10054
972 Ison, M.G., 2011. Antivirals and resistance: influenza virus. Curr. Opin. Virol. 1, 563–573.
973 https://doi.org/10.1016/j.coviro.2011.09.002

974 Iyengar, S., Farnham, P.J., 2011. KAP1 Protein: An Enigmatic Master Regulator of the Genome. J. Biol.
975 Chem. 286, 26267–26276. https://doi.org/10.1074/jbc.R111.252569
976 Javier, R.T., Butel, J.S., 2008. The History of Tumor Virology. Cancer Res. 68, 7693–7706.
977 https://doi.org/10.1158/0008-5472.CAN-08-3301
978 Jeffery, C.J., 2019. Multitalented actors inside and outside the cell: recent discoveries add to the number
979 of moonlighting proteins. Biochem. Soc. Trans. 47, 1941–1948.
980 https://doi.org/10.1042/BST20190798
981 Jeffery, C.J., 2018. Protein moonlighting: what is it, and why is it important? Philos. Trans. R. Soc. B Biol.
982 Sci. 373, 20160523. https://doi.org/10.1098/rstb.2016.0523
983 Jin, X., Pan, Y., Wang, L., Zhang, L., Ravichandran, R., Potts, P.R., Jiang, J., Wu, H., Huang, H., 2017.
984 MAGE-TRIM28 complex promotes the Warburg effect and hepatocellular carcinoma progression
985 by targeting FBP1 for degradation. Oncogenesis 6, e312–e312.
986 https://doi.org/10.1038/oncsis.2017.21
987 Kaján, G.L., Doszpoly, A., Tarján, Z.L., Vidovszky, M.Z., Papp, T., 2020. Virus–Host Coevolution with a
988 Focus on Animal and Human DNA Viruses. J. Mol. Evol. 88, 41–56.
989 https://doi.org/10.1007/s00239-019-09913-4
990 Krump, N.A., You, J., 2018. Molecular mechanisms of viral oncogenesis in humans. Nat. Rev. Microbiol.
991 16, 684–698. https://doi.org/10.1038/s41579-018-0064-6
992 Lingappa, U.F., Wu, X., Macieik, A., Yu, S.F., Atuegbu, A., Corpuz, M., Francis, J., Nichols, C., Calayag, A.,
993 Shi, H., Ellison, J.A., Harrell, E.K.T., Asundi, V., Lingappa, J.R., Prasad, M.D., Lipkin, W.I., Dey, D.,
994 Hurt, C.R., Lingappa, V.R., Hansen, W.J., Rupprecht, C.E., 2013. Host–rabies virus protein–protein
995 interactions as druggable antiviral targets. Proc. Natl. Acad. Sci. 110.
996 https://doi.org/10.1073/pnas.1210198110

997 Lingappa, V., Hurt, C., Garvey, E., 2013. Capsid Assembly as a Point of Intervention for Novel Anti-viral
998 Therapeutics. Curr. Pharm. Biotechnol. 14, 513–523.
999 https://doi.org/10.2174/13892010113149990201
1000 MacKinnon, A.L., Taunton, J., 2009. Target Identification by Diazirine Photo-Cross-Linking and Click
1001 Chemistry. Curr. Protoc. Chem. Biol. 1, 55–73.
1002 https://doi.org/10.1002/9780470559277.ch090167
1003 Malovannaya, A., Lanz, R.B., Jung, S.Y., Bulynko, Y., Le, N.T., Chan, D.W., Ding, C., Shi, Y., Yucer, N.,
1004 Krenciute, G., Kim, B.-J., Li, C., Chen, R., Li, W., Wang, Y., O'Malley, B.W., Qin, J., 2011. Analysis of
1005 the Human Endogenous Coregulator Complexome. Cell 145, 787–799.
1006 https://doi.org/10.1016/j.cell.2011.05.006
1007 Morales-Sánchez, A., Fuentes-Pananá, E., 2014. Human Viruses and Cancer. Viruses 6, 4047–4079.
1008 https://doi.org/10.3390/v6104047

1009 Motlagh, H.N., Hilser, V.J., 2012. Agonism/antagonism switching in allosteric ensembles. Proc.
1010 Natl. Acad. Sci. U. S. A. 109, 4134–4139. https://doi.org/10.1073/pnas.1120519109

1011

1012 Müller-Schiffmann, A., Michon, M., Lingappa, A.F., Yu, S.F., Du, L., Deiter, F., Broce, S., Mallesh, S.,
1013 Crabtree, J., Lingappa, U.F., Macieik, A., Müller, L., Ostermann, P.N., Andrée, M., Adams, O.,
1014 Schaal, H., Hogan, R.J., Tripp, R.A., Appaiah, U., Anand, S.K., Campi, T.W., Ford, M.J., Reed, J.C.,
1015 Lin, J., Akintunde, O., Copeland, K., Nichols, C., Petrouski, E., Moreira, A.R., Jiang, I., DeYarman,
1016 N., Brown, I., Lau, S., Segal, I., Goldsmith, D., Hong, S., Asundi, V., Briggs, E.M., Phyo, N.S.,
1017 Froehlich, M., Onisko, B., Matlack, K., Dey, D., Lingappa, J.R., Prasad, M.D., Kitaygorodskyy, A.,
1018 Solas, D., Boushey, H., Greenland, J., Pillai, S., Lo, M.K., Montgomery, J.M., Spiropoulou, C.F.,
1019 Korth, C., Selvarajah, S., Paulvannan, K., Lingappa, V.R., 2022. A Pan-respiratory Antiviral

1020 Chemotype Targeting a Transient Host Multiprotein Complex (preprint). Biochemistry.
1021 https://doi.org/10.1101/2021.01.17.426875
1022 Müller-Schiffmann, A., Torres, F., Kitaygorodskyy, A., Ramani, A., Alatza, A., Tschirner, S., Prikulis, I., Yu,
1023 S., Dey, D., Bader, V., Rozemuller, A., Wray, S., Gopalakrishnan, J., Riek, R., Lingappa, V.R., Korth,
1024 C., 2021a. Macrophage migration inhibitory factor is a valid drug target at the intersection of
1025 herpes simplex virus 1 replication and Alzheimer's disease-relevant cellular pathology (preprint).
1026 Microbiology. https://doi.org/10.1101/2021.09.11.459903
1027 Müller-Schiffmann, A., Trossbach, S.V., Lingappa, V.R., Korth, C., 2021b. Viruses as 'Truffle Hounds':
1028 Molecular Tools for Untangling Brain Cellular Pathology. Trends Neurosci. 44, 352–365.
1029 https://doi.org/10.1016/j.tins.2020.11.004
1030 Neo, S.H., Itahana, Y., Alagu, J., Kitagawa, M., Guo, A.K., Lee, S.H., Tang, K., Itahana, K., 2015. TRIM28 Is
1031 an E3 Ligase for ARF-Mediated NPM1/B23 SUMOylation That Represses Centrosome
1032 Amplification. Mol. Cell. Biol. 35, 2851–2863. https://doi.org/10.1128/MCB.01064-14
1033 OncoPanelTM Cell-Based Profiling Service Details, n.d. URL
1034 https://www.eurofinsdiscoveryservices.com/services/phenotypic-assays/oncopanel/oncopanel-
1035 details (accessed 8.9.22).
1036 O'Shea, C.C., 2005. Viruses: tools for tumor target discovery, and agents for oncolytic therapies – an
1037 introduction. Oncogene 24, 7636–7639. https://doi.org/10.1038/sj.onc.1209035
1038 Pfeffer, C., Singh, A., 2018. Apoptosis: A Target for Anticancer Therapy. Int. J. Mol. Sci. 19, 448.
1039 https://doi.org/10.3390/ijms19020448
1040 Priyamvada, L., Burgado, J., Baker-Wagner, M., Kitaygorodskyy, A., Olson, V., Lingappa, V.R.,
1041 Satheshkumar, P.S., 2021. New methylene blue derivatives suggest novel anti-orthopoxviral
1042 strategies. Antiviral Res. 191, 105086. https://doi.org/10.1016/j.antiviral.2021.105086

1043 Pucci, B., Kasten, M., Giordano, A., 2000. Cell Cycle and Apoptosis. Neoplasia 2, 291–299.
1044 https://doi.org/10.1038/sj.neo.7900101
1045 Randolph, K., Hyder, U., D'Orso, I., 2022. KAP1/TRIM28: Transcriptional Activator and/or Repressor of
1046 Viral and Cellular Programs? Front. Cell. Infect. Microbiol. 12, 834636.
1047 https://doi.org/10.3389/fcimb.2022.834636
1048 Reed, J.C., Solas, D., Kitaygorodskyy, A., Freeman, B., Ressler, D.T.B., Phuong, D.J., Swain, J.V., Matlack,
1049 K., Hurt, C.R., Lingappa, V.R., Lingappa, J.R., 2021. Identification of an Antiretroviral Small
1050 Molecule That Appears To Be a Host-Targeting Inhibitor of HIV-1 Assembly. J. Virol. 95, e00883-
1051 20. https://doi.org/10.1128/JVI.00883-20
1052 Reference ID" 4433223- Accessdata.fda.gov, n.d. URL
1053 https://www.accessdata.fda.gov/drugsatfda_docs/label/2019/020509s082lbl.pdf (accessed
1054 8.9.22).
1055 Reichel, A., Lienau, P., 2015. Pharmacokinetics in Drug Discovery: An Exposure-Centred Approach to
1056 Optimising and Predicting Drug Efficacy and Safety, in: Nielsch, U., Fuhrmann, U., Jaroch, S.
1057 (Eds.), New Approaches to Drug Discovery, Handbook of Experimental Pharmacology. Springer
1058 International Publishing, Cham, pp. 235–260. https://doi.org/10.1007/164_2015_26
1059 Singh, S., Singh, P., 2018. Pattern and impact of drugs targeted toward toxicity amelioration in patients
1060 receiving cancer chemotherapy. Perspect. Clin. Res. 9, 23.
1061 https://doi.org/10.4103/picr.PICR_156_16
1062 Tanaka, A., 2009. Identification of the Specific Binding Proteins of Bioactive Small Compound Using
1063 Affinity Resins, in: Koga, H. (Ed.), Reverse Chemical Genetics, Methods in Molecular Biology.
1064 Humana Press, Totowa, NJ, pp. 181–195. https://doi.org/10.1007/978-1-60761-232-2_14
1065 Usman, R.M., Razzaq, F., Akbar, A., Farooqui, A.A., Iftikhar, A., Latif, A., Hassan, H., Zhao, J., Carew, J.S.,
1066 Nawrocki, S.T., Anwer, F., 2021. Role and mechanism of autophagy-regulating factors in

1067 tumorigenesis and drug resistance. Asia Pac. J. Clin. Oncol. 17, 193–208.
1068 https://doi.org/10.1111/ajco.13449
1069 Wang, C., Ivanov, A., Chen, L., Fredericks, W.J., Seto, E., Rauscher, F.J., Chen, J., 2005. MDM2 interaction
1070 with nuclear corepressor KAP1 contributes to p53 inactivation. EMBO J. 24, 3279–3290.
1071 https://doi.org/10.1038/sj.emboj.7600791
1072 Wei, C., Cheng, J., Zhou, B., Zhu, L., Khan, Md.A., He, T., Zhou, S., He, J., Lu, X., Chen, H., Zhang, D., Zhao,
1073 Y., Fu, J., 2016. Tripartite motif containing 28 (TRIM28) promotes breast cancer metastasis by
1074 stabilizing TWIST1 protein. Sci. Rep. 6, 29822. https://doi.org/10.1038/srep29822
1075 Yang, Y., Fiskus, W., Yong, B., Atadja, P., Takahashi, Y., Pandita, T.K., Wang, H.-G., Bhalla, K.N., 2013.
1076 Acetylated hsp70 and KAP1-mediated Vps34 SUMOylation is required for autophagosome
1077 creation in autophagy. Proc. Natl. Acad. Sci. 110, 6841–6846.
1078 https://doi.org/10.1073/pnas.1217692110
1079 Yu, C., Zhan, L., Jiang, J., Pan, Y., Zhang, H., Li, X., Pen, F., Wang, M., Qin, R., Sun, C., 2014. KAP-1 is
1080 overexpressed and correlates with increased metastatic ability and tumorigenicity in pancreatic
1081 cancer. Med. Oncol. 31, 25. https://doi.org/10.1007/s12032-014-0025-5
1082

1083